



Characterization of a novel acidic phospholipase A₂ isolated from the venom of *Bothrops mattogrossensis*: From purification to structural modeling

Micaela de Melo Cordeiro Eulálio^{a,b}, Anderson Maciel de Lima^b,
Rodrigo Soares Caldeira Brant^c, Aleff Ferreira Francisco^b, Hallison Mota Santana^a,
Mauro Valentino Paloschi^a, Sulamita da Silva Setúbal^a, Carolina Pereira da Silva^a,
Milena Daniela Souza Silva^a, Charles Nunes Boeno^a, Anderson Makoto Kayano^{b,d},
Paula Helena Santa Rita^e, Leonardo de Azevedo Calderon^f, Andreimar Martins Soares^{b,g},
Daniela Priscila Marchi Salvador^h, Juliana Pavan Zuliani^{a,i,*}

^a Laboratory of Cellular Immunology Applied to Health, Oswaldo Cruz Foundation, FIOCRUZ Rondônia, Porto Velho, RO, Brazil

^b Laboratory of Protein Biotechnology and Bioactive Compounds (LABIOPROT), Oswaldo Cruz Foundation, FIOCRUZ Rondônia, Porto Velho, RO, Brazil

^c Carlos Chagas Institute (ICC), Mass Spectrometry Facility of FIOCRUZ Paraná, Curitiba, PR, Brazil

^d Center for Research in Tropical Medicine (CEPEM/SESAU-RO), Porto Velho, RO, Brazil

^e Bioterium of Dom Bosco Catholic University (UCDB), Campo Grande, MS, Brazil

^f Center for the Study of Biomolecules Applied to Health (CEBio), Oswaldo Cruz Foundation, FIOCRUZ Rondônia, Porto Velho, RO, Brazil

^g National Institute of Science and Technology of Epidemiology of Western Amazon, INCT-EpiAmO, Brazil

^h Toxic Protein Crystallography Laboratory (CPrTox-Lab), Federal University of Paraíba (UFPB), João Pessoa, PB, Brazil

ⁱ Department of Medicine, Federal University of Rondonia (UNIR), Porto Velho, RO, Brazil

ARTICLE INFO

Keywords:

Snake venom
Bothrops mattogrossensis
Phospholipase A₂
Endothelial cells

ABSTRACT

Phospholipases A₂ (PLA₂s) are highly prevalent in *Bothrops* snake venom and play a crucial role in inflammatory responses and immune cell activation during envenomation. Despite their significance, the specific role of PLA₂s from *Bothrops mattogrossensis* venom (BmV) in inflammation is not fully understood. This study sought to isolate and characterize a novel acidic PLA₂ from BmV, designated BmPLA₂-A, and to evaluate its effects on human umbilical vein endothelial cells (HUVECs), with a specific focus on cytotoxicity, adhesion, and detachment. BmPLA₂-A was isolated through a multi-step chromatographic procedure, involving cation exchange (CM-Sephrose), hydrophobic interaction (n-butyl-Sepharose-HP), and reversed-phase (C-18) chromatography. SDS-PAGE analysis revealed a single protein band of approximately 15 kDa. The primary structure of BmPLA₂-A was determined by LC-MS/MS, while its tertiary structure was modeled using AlphaFold. Enzymatic activity was verified with the synthetic substrate 4N3OBA. Molecular dynamics simulations were conducted to further investigate the catalytic mechanism of BmPLA₂-A at the molecular level. In vitro assays on HUVECs revealed that BmPLA₂-A neither induce cytokine release (IL-6, IL-8, IL-1β, TNF) nor affected cell viability, adhesion, or detachment. The characteristics of BmPLA₂-A are consistent with those of acidic Asp-49 PLA₂ enzymes, highlighting its potential involvement in the cytotoxic and inflammatory effects of the venom.

1. Introduction

Ophidian envenomation present a significant global public health concern, particularly in tropical and subtropical regions where snake diversity is highest [1]. Such envenomations are associated with a range of clinical complications, including tissue damage, hemostatic disorders,

and systemic alterations, which can lead to morbidity and even mortality. It is estimated that approximately 5 million ophidian accidents occur worldwide annually, leading to around 125,000 deaths [2–4].

Among the snakes implicated in these incidents, the genus *Bothrops*, part of the Viperidae family, is widely distributed across Central and South America and includes several species recognized for their

* Corresponding author at: Laboratório de Imunologia Celular Aplicada à Saúde – Fundação Oswaldo Cruz, Rua da Beira, 7671, CEP 76812-245 Porto Velho, RO, Brazil.

E-mail address: juliana.zuliani@fiocruz.br (J.P. Zuliani).

<https://doi.org/10.1016/j.ijbiomac.2024.139217>

Received 5 July 2024; Received in revised form 23 December 2024; Accepted 24 December 2024

Available online 26 December 2024

0141-8130/© 2024 Elsevier B.V. All rights reserved, including those for text and data mining, AI training, and similar technologies.

venomous potential [5]. *Bothrops mattogrossensis* is one of the species within this genus that contributes to ophidian accidents in Brazil. Envenomation by this species can lead to severe clinical complications and require immediate medical intervention [6].

Snake venoms are complex blends of proteins and bioactive peptides that play crucial roles in predation, defense, and prey digestion [7]. Among the various protein classes present in *Bothrops* venoms, phospholipases A₂ (PLA₂s) are prominent components responsible for many of the toxic effects observed in envenomation cases [8]. These PLA₂s have been extensively studied due to their clinical relevance and therapeutic potential, demonstrating their ability to interact with different cellular targets and biological systems, thereby triggering a cascade of pathological events. PLA₂s are enzymes acting by hydrolyzing phospholipids in cell membranes, triggering a series of harmful effects such as cell destruction, local inflammation, hemostatic disorders, and tissue necrosis [9,10]. However, significant knowledge gaps remain regarding the structural properties, mechanisms of action, and potential therapeutic applications of these enzymes.

Recent studies have underscored the importance of acidic PLA₂s across various species within the genus *Bothrops*, which are widely distributed throughout Central and South America. These acidic PLA₂s display a broad range of biochemical and toxicological properties, contributing to the venom's overall composition and pathogenicity of these snakes. For instance, acidic PLA₂s isolated from *Bothrops pirajai*, *Bothrops jararacussu*, *Bothrops leucurus*, *Bothrops moojeni* and *Bothrops pauloensis* have been shown to induce significant inflammatory responses, myotoxicity and alterations in hemostasis (Table 1). Moreover, the structural characterization of these enzymes has revealed conserved motifs that are crucial for their enzymatic activity, although species-specific variations exist, influencing their biological effects [38,40,48–51]. Despite these advances, the precise mechanisms of PLA₂s interaction with cellular targets, and the broader implications of their activities in envenomation, remain subjects of ongoing investigation.

In the present study, a novel acidic PLA₂ from *Bothrops mattogrossensis* snake venom was isolated and designated as BmPLA₂-A, and its biochemical and functional properties were described. Additionally, the action of BmPLA₂-A on Human Umbilical Vein Endothelial Cells (HUVECs) through viability assay (MTT), immunofluorescence, cell adhesion and detachment, and cytokine quantification (IL-1b, IL-6, IL-8, and TNF-α) were characterized.

2. Materials and methods

To accomplish the objectives of this study, a comprehensive experimental approach was implemented. The initial phase encompassed the isolation and biochemical characterization of phospholipase A₂ (PLA₂) from *Bothrops mattogrossensis* snake venom through the application of multiple chromatography techniques, including ion exchange, hydrophobic interaction, and reverse-phase chromatography. The purified

PLA₂ underwent extensive molecular characterization employing sodium dodecyl sulfate-polyacrylamide gel electrophoresis (SDS-PAGE), proteomic analysis via mass spectrometry, and computational modeling of its interaction with specific substrates. The biological effects of the isolated PLA₂ were subsequently assessed using a suit of in vitro assays conducted on human umbilical vein endothelial cells (HUVECs). These analyses focused on evaluating cytotoxicity, cell adhesion and detachment, as well as cytokine release. To further investigate the influence of PLA₂ on cellular behavior and the production of inflammatory mediators, advanced analytical techniques, including immunofluorescence microscopy and enzyme-linked immunosorbent assays (ELISA), were employed. Lastly, statistical analyses were conducted to ensure the validity and significance of the experimental findings, thereby reinforcing the reliability of the conclusions drawn from the study.

2.1. *Bothrops mattogrossensis* snake venom

Bothrops mattogrossensis venom was supplied by the Bioterium of the Catholic University Dom Bosco (UCDB), located in Campo Grande, Mato Grosso do Sul, Brazil, and stored under refrigerated conditions at the Bank of Amazonian Venoms at the Laboratory of Biotechnology of Proteins and Bioactive Compounds – FIOCRUZ-RO (authorization: Sis-Gen n° AFCAB61 and IBAMA 718.682).

2.2. Isolation of PLA₂ from *B. mattogrossensis* venom

2.2.1. Ion exchange chromatography (IEC)

Approximately 50 mg of *B. mattogrossensis* venom was dissolved in 1 mL of ammonium bicarbonate (NH₄HCO₃ – AMBIC) 50 mM, pH 8.0 (buffer A) and submitted to centrifugation at 3500 xg for 5 min to remove insoluble material. The resulting supernatant was subjected to fractionation using a CM-Sepharose FF® column (10 × 30 cm – GE Healthcare Life Science), which had been pre-equilibrated with buffer A. Fraction elution was carried out under a gradient of 0–100 % of AMBIC 500 mM, pH 8.0 over 5 column volumes, at a flow rate of 1 mL/min, utilizing an Akta Purifier Chromatography system (GE Healthcare Life Science). The elution process was monitored at 280 nm, and the manually collected fractions were subsequently lyophilized and stored at –20 °C.

2.2.2. Sodium dodecyl sulfate-polyacrylamide gel electrophoresis (12.5 % SDS-PAGE)

The relative molecular mass of the proteins was determined using the protocol established by Laemmli (1970) [11]. The samples were diluted in 10 µL of SDS buffer (consisting of Tris-HCl 0.5 M, pH 6.8; SDS 10 %; glycerol 100 %; β-mercaptoethanol; ultrapure H₂O and bromophenol blue), incubated for 5 min at 95 °C and then applied to the gel. After the run procedure, the gel was washed with deionized water and fixed in an aqueous solution of ethanol 50 % and acetic acid 12 % for 30 min. Subsequently, the gel was stained for 30 min with slight agitation in

Table 1
Acidic PLA₂ present in the venoms of other members of the genus *Bothrops*.

Snake Species	Acidic PLA ₂ Designation	Key Biological Effects	References
<i>Bothrops pirajai</i>	BpirPLA ₂ -I	Induces hypotension in vivo, phospholipolytic activity on artificial substrates, and inhibits platelet aggregation in vitro.	Teixeira et al., 2011 [38]
<i>Bothrops jararacussu</i>	BthA-I-PLA ₂	Non-toxic but induces time-independent edema (inhibited by EDTA), causes hypotension, and inhibits platelet aggregation.	Andrião-Escarso et al., 2002 [40]
<i>Bothrops leucurus</i>	BI-PLA ₂	Induces low myotoxicity and edema. Increases levels of proinflammatory cytokines (IL-12p40, TNF-α, IL-1β, IL-6) in human PBMCs, with no change in IL-8 and IL-10.	Nunes et al., 2011 [48]
<i>Bothrops moojeni</i>	BmooPLA ₂	High phospholipase activity, bactericidal effect, moderate cytotoxicity, and inhibits platelet aggregation. Also induces edema and hypotension.	Silveira et al., 2012 [49]
<i>Bothrops pauloensis</i>	BpPLA ₂ -TXI	Inhibits platelet aggregation, induces edema, and causes myotoxicity.	Ferreira et al., 2013 [50]
<i>Bothrops pauloensis</i>	Bp-PLA ₂	Displays indirect hemolytic activity, inhibits platelet aggregation, and induces edema and myotoxicity in vivo.	Rodrigues et al., 2007 [51]

PhastGel™ Blue R solution (GE Healthcare Life Science). Excess dye was removed by immersion in a bleach solution containing ethanol 20 % and acetic acid 3 %. Gel documentation was performed using a LabScan® scanner (GE Healthcare Life Science).

2.2.3. Hydrophobic interaction chromatography (HIC)

This procedure was conducted according to the method as described by Sobrinho et al. (2018) [12]. The CM1 fraction, diluted in buffer A (AMBIC 20 mM, pH 8.0 + NaCl 4 M), was applied to an n-butyl-Sepharose-HP® column (1 × 15 cm, GE Healthcare Life Science). Elution was carried out under a segmented gradient, with decreasing concentrations of NaCl in buffer B (AMBIC 20 mM), and a final step using deionized water, under a flow of 1 mL/min in an Akta Purifier chromatography system (GE Healthcare Life Science). Elution was monitored at 280 nm, and the fractions eluted in water were manually collected. These fractions were subsequently lyophilized and stored at -20 °C. The relative molecular masses of the eluted proteins were determined using 12.5 % SDS-PAGE, following the procedures outlined in Section 2.2.2.

2.2.4. Reverse-phase chromatography (RPC)

To ensure the highest degree of purity, the fraction eluted in water, from HIC, was subjected to reversed-phase chromatography (RPC) in a column (25 × 4.6 mm – Kinetex red), previously equilibrated with solution A [trifluoroacetic acid (TFA, 0.1 %)] and eluted under a gradient of 0–70 % of solution B [acetonitrile (ACN, 99.9 %) and TFA 0.1 %] in 10 column volumes, at a flow rate of 1 mL/min. Elution was monitored at 280 nm and the manually collected fraction was lyophilized in a Speed Vac and stored at -20 °C. PLA₂ activity was measured as described in Section 2.3.1. The apparent molecular mass of the eluted protein was determined using 12.5 % SDS-PAGE, following the procedures outlined in Section 2.2.2.

2.3. Biochemical characterization

2.3.1. Phospholipase activity with 4-nitro-3 (octanoyloxy) benzoic acid (4N3OBA)

The procedure was carried out as described by Petrovic et al. (2001) [13], with modifications. Initially, 5 mg of 4N3OBA was diluted in 5.4 mL of ACN. Aliquots of 0.1 mL were dried using a vacuum evaporator concentrator and stored at -20 °C. The 4N3OBA aliquot was diluted in 1.2 mL of sample buffer (Tris-HCl 10 mM, pH 8.0; CaCl₂ 10 mM, and NaCl 100 mM) and kept on ice. Phospholipase activity was carried out with 190 µL of the 4N3OBA along with 10 µg of the samples under evaluation applied in triplicate. After sample addition, absorbance was measured at 425 nm using an Eon microplate spectrophotometer (Biotek) at 37 °C during a 30 min incubation period.

2.3.2. Theoretical isoelectric point (pI)

The theoretical isoelectric point was determined using the ExPasy ProtParam tool [14]. The protein sequence, obtained from LC-MS (see item 2.3.3) analysis, was entered into the ProtParam tool, which provided detailed information on various physicochemical properties.

2.3.3. LC-MS and LC-MS/MS analysis

The sample preparation for peptide mapping included drying in Speed Vac (Thermo Fisher) 45 µg of protein, then resuspended in 40 µL of urea 6 M, reduced with DTT, and alkylated with Iodoacetamide before dividing the sample into three tubes for digestion with different proteases (trypsin, pepsin, and GluC) overnight. Subsequently, the samples were desalinated with an in-house made C18 Stage-tip. LC-MS/MS analyses of the proteolytic digestions were conducted at the Mass Spectrometry Facility RPT02H/ Carlos Chagas Institute – Fiocruz Paraná. The runs were performed on an Ultimate 3000 nLC coupled with an Orbitrap Exploris 120 Mass Spectrometer (Thermo Fisher Scientific). Peptide separation was achieved using an in-house packed C18-AQ analytical column with 75 µm ID and 15 cm length, and data-

dependent acquisition mode with top 4 ions selected for MS² was employed with 120,000 and 15,000 resolutions for MS¹ and MS², respectively. Peptide mapping and database identification were performed using PEAKS Studio x PRO. Several analyses were conducted. Firstly, peptide de novo sequencing and database identification were performed using a database containing several phospholipases sequences. Subsequently, the database was set with the proteins described in NCBI for the genus *Bothrops* and after, two sequences with high coverage, identified as acidic phospholipases, were selected and used as a database with two entries. These sequences also served as templates for de novo protein assembly by Stitch [15]. Search parameters, including parent and fragment mass error tolerance, enzyme specificity, and modifications were adjusted according to experimental conditions. LC-MS intact mass analysis was performed on the same Mass Spectrometer and Chromatograph described for peptide mapping. Separation was carried out on mAb Pack (Thermo Fisher) with 3 mm of ID and 100 mm of length MS¹ acquisition with 60,000 resolution. Deconvolution of chromatographic peaks were performed using Unidec [16].

2.3.4. Computational analysis of BmPLA₂-A interaction with dilaurylphosphatidylcholine

The structure of *Bothrops mattogrossensis* PLA₂ (BmPLA₂-A) was retrieved from the AlphaFold Protein Structure Database (entry: I2DAL5). Molecular docking between BmPLA₂-A and its substrate Dilaurylphosphatidylcholine (CID:65262) was performed using Autodock Vina [17], with the parameters set to Exhaustiveness and Nun modes at 80 and 90, respectively, with a grid center at X:7,44; Y:0,48; Z:-2496, and dimensions of X: 34,134; Y:28,072; 31,563. The predicted BmPLA₂-A + Ca²⁺+DLPC was subjected to a binding affinity prediction using the PRODIGY web server [18]. Next, the BmPLA₂-A + Ca²⁺+DLPC native complex was protonated at pH 7 using APBS-PDB2PQR webserver [19] and subjected to molecular dynamics using GROMACS 2024 [20] employing the CHARMM36-mar2019 force field [21]. The simulations were conducted with a neutral net charge box 1,5 Å from the farthest atom, solvated with TIP3P water, and equilibrated with 150 mM CaCl₂. The system underwent energy minimization using the Steepest Descent algorithm until the energy dropped below 1000 kJ/mol/nm. Equilibration followed under an isochoric-isothermal (NVT) ensemble for 1 ns, generating velocities according to the Maxwell-Boltzmann distribution at 298.15 K using the V-Rescale thermostat [22] followed by an isothermal-isobaric (NPT) ensemble using the Berendsen barostat at 1 bar [23]. An unrestrained 150 ns simulation was then executed using the Nose-Hoover Thermostat and Parrinello-Rahman barostat [24,25]. Nonbonded interactions were calculated within a radius of 12 Å using a switching function between 10 and 12 Å. Afterwards, the trajectories were analyzed, and the radius of gyration (Rg) and backbone root-mean-square deviation (RMSD) measurements were extracted from the main interacting parties for stability assessment. Next, the trajectories were subjected to clusterization using the Gromos method with an RMSD distribution of 2 Å [26]. Root-mean-square fluctuation (RMSF) was calculated to assess residue-level flexibility, identifying critical regions of flexibility and stability throughout the protein. PyContact performed contact analysis and solvent-accessible surface area (SASA) evaluation [27]. All the images and interaction maps were made with UCSF ChimeraX and LIGPLOT+ 40,41 [28,29].

2.4. Cytotoxicity, adhesion, detachment, and release of cytokines of human umbilical vein endothelial cells (HUVECs) under the actions of BmPLA₂-A

2.4.1. Human umbilical vein endothelial cells (HUVEC) cell lineage culture

The HUVEC cell line (CRL-1772ATCC) was generously provided by Dr. Gustavo Pereira from UNIFESP, Brazil. The cells were cultured in a growth medium consisting of Dulbeccos Modified Eagles Medium (DMEM, Invitrogen), supplemented with 10 % heat-inactivated fetal

bovine serum and 1 % antibiotic-antimycotic solution in a humidified atmosphere of 5 % CO₂ at 37 °C. The growth medium was refreshed every two days. Once the cell monolayer sub-confluent, the cells were washed with 1 × phosphate-buffered saline (PBS; 140 mM NaCl; 2.5 mM KCl; 8 mM Na₂HPO₄; 1.4 mM KH₂PO₄; pH 7.4) and detached using a 1 × trypsin solution (0.05 % trypsin and 0.02 % EDTA). The detached cells were then centrifuged at 600 ×g for 5 min, resuspended in 1 mL of DMEM, and prepared for subsequent assays as described to Santana et al., (2024) [30].

2.4.2. Viability, adhesion, and detachment

For the viability, adhesion, and cell detachment assay, HUVECs were plated in 96-well plates and incubated with BmPLA₂-A at various concentrations (3.125, 6.25, 12.5, 25, and 50 µg/mL) at different time intervals. Subsequently, 10 µL of MTT (5 mg/mL) was added and incubated for 1 h. After incubation, the cells were centrifuged (400 ×g for 5 min) again and the supernatant containing unreduced MTT was removed. Then, 100 µL of DMSO was added to solubilize the formazan crystals. The degree of reduction of MTT to formazan was quantified by measuring the optical density (OD) at 570 nm using a BioTek Synergy HT Multi-Detection spectrophotometer.

HUVEC adhesion was assayed according to the procedure described by Setúbal et al. (2011) [31] and Santana et al. (2024) [30]. The cells (2 × 10⁵ cells/well) were cultured for 30 min and 1 h with DMEM (control) or BmPLA₂-A (3.1 to 50 µg/mL) diluted in DMEM at 37 °C in a humidified atmosphere (5 % CO₂). After incubation, the plates were washed three times with PBS and the adherent cells were fixed with methanol. After staining with 0.1 % Giemsa solution for 40 min, the plates were washed with water, and the remaining dye was solubilized with methanol. Absorbance was determined spectrophotometrically at 550 nm. The control group was considered 100 %.

HUVEC detachment was conducted according to the procedure described by Setúbal et al. (2011) [31] and Santana et al. (2024) [30]. The cells (2 × 10⁵/well) were plated on 96-well and allowed to attach for 24 h at 37 °C in a humidified atmosphere (5 % CO₂). The adhered HUVEC were incubated with DMEM (control), or BmPLA₂-A (3.1 to 50 µg/mL) diluted in DMEM for 30 min and 1 h at 37 °C in a humidified atmosphere (5 % CO₂). After incubation, the procedure was carried out as previously mentioned for adhesion. After that, the cells were imaged using a 10× magnification benchtop optical microscope.

For immunofluorescence assay, HUVECs (2 × 10⁵ per well) diluted in DMEM supplemented with 10 % FBS were plated onto 24-well plates on coverslips and incubated overnight at 37 °C, 5 % CO₂. Subsequently, the cells were incubated for 1 h with BmPLA₂-A (50 µg/mL) and/or DMEM (control). After incubation, the cells were fixed in 4 % paraformaldehyde and washed in PAB [PBS + 5 mg/mL BSA and 0.5 mg/mL sodium azide (NaN₃)]. Thereafter, the cells were permeabilized with acetone PA, and subsequently, Alexa FluorTM 546 Phalloidin (1:40) diluted in PAB + 10 % FBS was added for 20 min in the dark. Slips were mounted in Fluoromount-GTM and the images were then captured using Nikon Eclipse Ti Confocal inverted microscope and were collected using constant automatic gain among the samples to quantify the differences in the absolute levels of fluorescence intensities under different conditions. Ten fields of view of each condition were observed impartially. The acquired images were subsequently analyzed using the ImageJ software (National Institutes of Health) to quantify the absolute total fluorescence intensity. The calculated fluorescence intensity of the fields of view was plotted as the mean normalized intensity for the total number of cells [32].

2.4.3. IL-6, IL-8, TNF-α and IL-1β quantifications

IL-6, IL-8, TNF-α, and IL-1β quantifications were performed using enzyme immunoassay (EIA) in supernatants collected from the previous experiments (MTT and detachment) using Human DuoSet ELISA from R&D Systems (Oxon, UK) specific cytokines kits following the manufacturer's instructions.

2.5. Statistical analysis

The statistical analysis was conducted using GraphPad Prism version 5. The data were expressed as mean ± standard error, followed by Tukey's post-hoc test for sample comparisons. A *P*-value of <0.05 was considered statistically significant.

3. Results

3.1. Purification of BmPLA₂-A

The chromatographic procedures employed for the isolation of BmPLA₂-A, a novel PLA₂ of *Bothrops mattogrossensis*. The isolation involved three distinct chromatographic techniques: first, ion exchange chromatography was performed using a CM-Sepharose column (supplementary material 1); second, hydrophobic interaction chromatography utilizing an n-butyl-Sepharose-HP column (supplementary material 2); lastly, reverse-phase chromatography utilizing a C18 Kinetex column (Fig. 1A). The resulting BmPLA₂-A, derived from the venom of *B. mattogrossensis*, exhibited a high level of purity, as confirmed by SDS-PAGE analysis (Fig. 1A).

3.2. Biochemical characterization of BmPLA₂-A

A comprehensive characterization of the novel phospholipase A₂, BmPLA₂-A, isolated from *Bothrops mattogrossensis* venom, is comprehensively provided. The characterization encompasses multiple analytical approaches. The purity and molecular weight of the protein were assessed using SDS-PAGE, while its physicochemical properties were inferred from its primary amino acid sequence. The enzymatic activity of BmPLA₂-A was quantified through phospholipase specific assays. To further elucidate its properties, advanced proteomic techniques, such as LC-MS and peptide mapping, were employed to determine the protein's sequence similarity to known homologs. Structural analyses and molecular modeling provided insights into its three-dimensional structure, evolutionary conservation, and substrate interaction dynamics. Furthermore, molecular dynamics simulations elucidated the enzyme's stability and flexibility during catalysis, shedding light on its functional mechanisms.

As part of the comprehensive characterization, 12.5 % sodium dodecyl sulfate-polyacrylamide gel electrophoresis (SDS-PAGE) was performed following each chromatographic step to evaluate the molecular weight and assess the purity of the protein fractions (supplementary material 1, 2 and Fig. 1A). This analysis confirmed that BmPLA₂-A achieved homogeneity, as evidenced by an apparent molecular mass of 15,000 Da in the presence of the reducing agent (Fig. 1A).

To determine the pI, was utilized the ExPASy ProtParam tool, which provided various physicochemical properties of BmPLA₂-A, deduced from its primary structure composed by 122 amino acid residues, including its molecular weight of 13,635.18 Da, and a theoretical isoelectric point (pI) of 4.91 (Table 2). The amino acid composition reveals a significant presence of cysteine (11.5 %), glycine (10.7 %), and aspartic acid (8.2 %), with the remaining amino acids contributing in varying smaller proportions. The protein has a total of 17 negatively charged residues (Asp + Glu) and 13 positively charged residues (Arg + Lys). Its atomic composition is represented by the molecular formula C₅₈₄H₈₆₈N₁₆₀O₁₈₉S₁₅, totaling 1.816 atoms. The estimated half-life of the protein is 1.4 h in mammalian reticulocytes in vitro, 3 min in yeast in vivo, and over 10 h in *Escherichia coli* in vivo. The instability index of 34.94 classifies the protein as stable, while its aliphatic index is 39.92. The grand average of hydropathicity (GRAVY) is -0.608, indicating a hydrophilic nature.

In addition, experiments were conducted to evaluate the phospholipase activity of BmPLA₂-A. For this purpose, a lipid substrate (4N3OBA) was employed, which was hydrolyzed under the action of phospholipases, resulting in complete conversion to the chromophore,

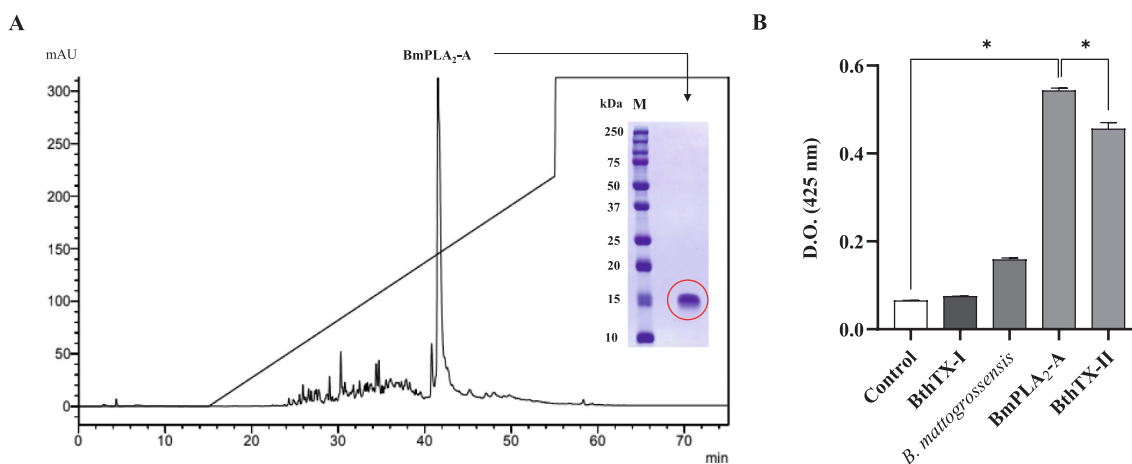


Fig. 1. (A) Final chromatographic purification of BmPLA₂-A using reverse-phase chromatography on a C18 column (25 mm × 4.6 mm, Kinetex RED). The elution gradient ranged from 0 % to 70 % of a buffer containing 99.9 % acetonitrile and 0.1 % trifluoroacetic acid (TFA), with a flow rate of 1 mL/min and monitoring at 280 nm. The collected fraction was analyzed by 12.5 % SDS-PAGE. M: Molecular weight marker. The BmPLA₂-A protein band is highlighted in red. (B) Phospholipase activity assay of BmPLA₂-A, evaluated by hydrolysis of the lipid substrate 4-nitro-3-octanoyloxybenzoic acid (4N3OBA), leading to the release of a nitro group, measured at 425 nm. Negative controls included H₂O and BthTX-I (a phospholipase lacking catalytic activity). BthTX-II, a phospholipase with known catalytic activity, served as a positive control. The catalytic activity assay (B) was performed using the fraction purified in (A). Statistical significance is indicated by an asterisk (*).

Table 2

Physicochemical properties of BmPLA₂-A: number of amino acids, molecular weight (KDa), theoretical isoelectric point (pI), and instability index.

Number of amino acids	Molecular weight	Theoretical pI	Instability index
122	13,635.18	4.91	34.94

4-nitro-3-hydroxy-benzoic acid, which could be quantified by spectrophotometry at 425 nm (Fig. 1B). For the assessment of the BmPLA₂-A phospholipase activity, negative controls (H₂O and BthTX-I, a PLA₂-Lys49 from *B. jararacussu* venom), and positive control (BthTX-II, a PLA₂-Asp49 from *B. jararacussu* venom), as well as *B. matogrossensis* venom, were employed. Notably BmPLA₂-A exhibited a catalytic activity superior to that observed in the positive control (Fig. 1B), represented by BthTX-II, a PLA₂ previously characterized from the *B. jararacussu* venom, whose activity is well-established and recognized [33].

The LC-MS analysis of the purified intact protein, illustrated in the Total Ion Chromatogram (TIC) in Fig. 2A, demonstrated a well-defined

retention time window corresponding to the BmPLA₂-A protein, thereby confirming the protein's purity and consistency. The deconvoluted mass spectra (Fig. 2B) revealed three predominant peaks (A, B, and C), each representing specific molecular species of the purified protein, as detailed in Table 3. Peptide mapping data, using the genus *Bothrops* database, showed high similarity between the sequence of BmPLA₂-A and AFJ79208.1 acidic secretory phospholipase A₂ (sPLA₂-II) from *Bothrops diporus* snake venom. In the trypsin digestion, AFJ79208.1 was the protein with the highest intensity among the 129 identified. For pepsin and GluC digestion, it ranked second in intensity, falling behind

Table 3

Details of the deconvoluted peaks from the LC-MS analysis of BmPLA₂-A.

Mass	Area (% of total)	Total Area	Label	Deconvolution score
13,591.53	42.00	6.22E+07	A	0.96
13,677.55	45.00	6.67E+07	B	0.97
13,809.29	13.00	1.93E+07	C	0.98

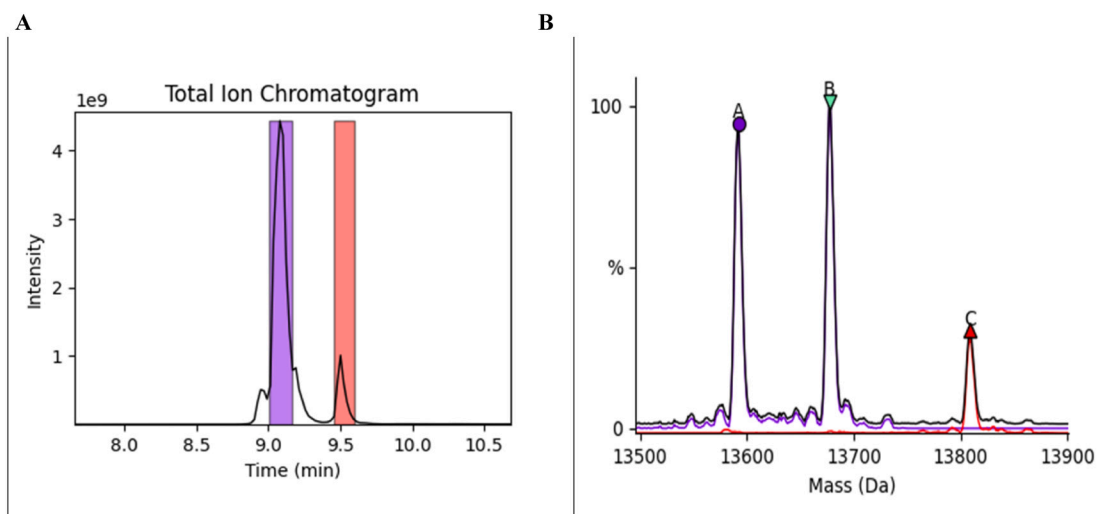


Fig. 2. (A) Total Ion Chromatogram (TIC) of BmPLA₂-A obtained by liquid chromatography-mass spectrometry (LC-MS). (B) Deconvoluted Peaks of Intact mass analysis of BmPLA₂-A.

the protein C9DPL5.1 acidic phospholipase A₂ BpirPLA₂-1 from *Bothrops pirajai* snake venom, however, C9DPL5.1 had only 45 % of its sequence covered (supplementary material 3).

The PSM analysis against the database containing 15 phospholipase sequences from *Bothrops* demonstrated 100 % protein coverage of AFJ79208.1, and AFJ79207.1, both sequences related to *Bothrops diporus* snake venom and with a difference of only 4 amino acids and 30 Da between the two proteins (Fig. 3). Table 4 presents the PSM data from the three digestions and the corresponding identification of these proteins. To further validate the data and infer which sequences are the most likely to be in the sample, de novo sequencing with peptides generated from PEAKS studio x Pro was assembled into proteins with Stitch [15].

A new database was created, incorporating the template and consensus sequences generated by de novo sequencing. A third PSM analysis was then performed using these sequences, along with an un-specific post-translational modifications search with PEAKS PTM algorithm and possible aminoacidic mutations with PEAKS SPIDER algorithm. PEAKS DB demonstrated 100 % protein coverage for both AFJ79208.1 and AFJ79207.1, for these two sequences were selected for further analysis. AFJ79208.1 and AFJ79207.1 molecular formulas were calculated with ChemCalc [34], and their molecular weight were calculated based on the formula to generate Table 5.

In this study, the PLA₂ from *B. matogrossensis* (BmPLA₂-A) was identified and found to possess an identical sequence to the PLA₂ from *Bothrops diporus*. This discovery prompted further structural and functional analyses. The three-dimensional structure of the BmPLA₂-A was approximated using the high-confidence model of *B. diporus* PLA₂ available in the AlphaFold Protein Database, reflecting a per-residue model confidence score (pLDDT) indicative of reliable structural prediction.

To elucidate the evolutionary and functional context of BmPLA₂-A, a multiple sequence alignment (MSA) was performed using the BLAST protein web server, highlighting the conservation and variation of this enzyme among various snake species. The alignment included 15 closely related homologs that displayed >80 % identity, underscoring the conserved nature of this enzyme across different species (Fig. 4). The structural superimposition of BmPLA₂-A with these homologs showed an RMSD across all 122 pairs of aligned atoms of 0.462 Å, indicating high structural similarity (Fig. 4).

Subsequent molecular docking analyses were performed to investigate the interaction between BmPLA₂-A and its natural substrate, Dilaurylphosphatidylcholine (DLPC). The docking results predicted a high-affinity binding mode, with the substrate engaging critical catalytic residues located within the enzyme's hydrophobic channel. This interaction was characterized by a binding free energy (ΔG) of -10.87 kcal/mol, suggesting a strong and specific interaction conducive to effective catalysis (Fig. 4).

Moreover, molecular dynamics (MD) simulations were performed to assess the stability and dynamics of the native complex comprising BmPLA₂-A + Ca²⁺ + DLPC. The simulations replicated conditions optimal for catalytic activity, maintaining a temperature of 25 °C, a pH of 7, and a concentration of 0.15 mM CaCl₂. One hundred fifty nanoseconds of simulation were performed in duplicates, generating 300 ns of trajectory for the enzyme-substrate complex. The trajectories were analyzed independently, with particular attention given to the RMSD of DLPC, as well as the RMSD, Rg, and RMSF of BmPLA₂-A.

The RMSD of BmPLA₂-A exhibited a gradual increase, stabilizing around 0.2–0.3 nm, which suggests that the enzyme undergoes initial adjustments upon substrate binding but maintains its overall structural integrity throughout the simulation. The Rg values oscillate around 1.5 nm, which indicates the enzyme's compactness and overall stability. The RMSD of DLPC fluctuates between 0.2 and 0.6 nm, suggesting that while there are some conformational changes in the substrate during the simulation, it remains relatively stable within the binding site.

To further investigate the flexibility of the BmPLA₂-A enzyme, RMSF analysis was performed to evaluate the dynamic behavior of each individual residue. As illustrated in Fig. 5, the analysis revealed that the most flexible regions correspond to residues 70–73, where RMSF values peaked at 0.43 nm. These residues are located within loop and are surface-exposed, thereby exhibiting increased flexibility. In contrast, residues of the active site, particularly Asp49, His48, and Tyr52, displayed lower RMSF values (approximately 0.05 to 0.2 nm) than the rest of the enzyme. This region's stability is critical for maintaining the integrity of the enzyme's catalytic core, which includes the Ca²⁺ ion.

Furthermore, a cluster analysis was performed with a concatenated trajectory comprising both replicas to elucidate the most predominant conformations of BmPLA₂-A in solution. The analysis generated 12 clusters, with the central structures of each cluster representing pivotal stable states of the enzyme in complex with Ca²⁺ and DLPC. These central conformations provide insight into the dynamic behavior and structural adaptations that occur within BmPLA₂-A during the catalytic process (Fig. 5).

The interactions between BmPLA₂-A, DLPC, and Ca²⁺ were meticulously analyzed over a 300 ns of the concatenated replicas using a comprehensive contact analysis (Fig. 6). Panel A presents the structural representation of the BmPLA₂-A enzyme bound to Ca²⁺ and DLPC, highlighting critical interactions with Ca²⁺ and catalytic residues. Panel B provides a detailed view of the DLPC molecule, emphasizing the atom positioning and numbering. Panel C underscore the sustained and robust interactions between Ca²⁺ and the phosphate group of DLPC, with solid contacts noted at oxygen 13 (O13). Additional atoms, such as oxygen 22 (O22) and carbon 21 (C21), also displayed elevated mean interaction scores, further reinforcing the pivotal role of Ca²⁺ in stabilizing the substrate within the enzyme's active site. Panel D illustrates the solvent-accessible surface area (SASA) of DLPC fluctuated throughout the 300 ns

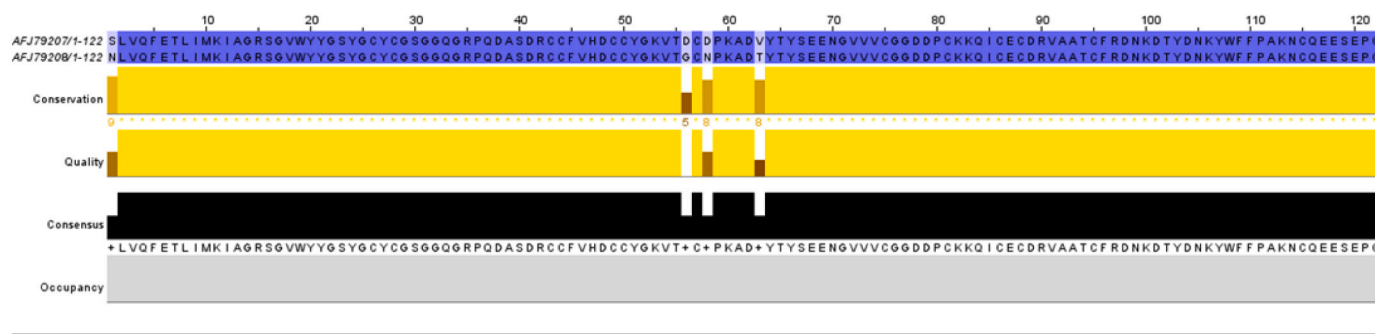


Fig. 3. Computational Analysis of BmPLA₂-A. The top panel features a multiple sequence alignment, highlighting PLA₂ enzymes that share over 80 % identity with BmPLA₂-A, emphasizing evolutionary conservation across species. In the bottom left, the three-dimensional structure of BmPLA₂-A is superimposed against the structures of all PLA₂s included in the sequence alignment, illustrating the highly conserved fold. In the lower center and right side, the docked structure of BmPLA₂-A with its natural substrate, DLPC, is displayed, showcasing fundamental interactions critical for substrate binding and enzymatic activity.

Table 4

PEAKS DB results of analysis with the sequences of AFJ79208.1 and AFJ79207.1.

	#Scans			#Features	Identified			#Peptides	#Sequences
	MS1	MS/MS	#Chimera		#PSMs	#Scans	#Features*		
Trypsin	34,381	55,214	15,552	97,197	4947	4482	2450	812	540
GluC	35,132	49,806	19,544	129,561	2646	2307	1592	522	321
Pepsin	34,813	52,146	12,892	100,068	2738	2603	1736	570	396

* Features are identified by DB search only.

Table 5Information of the sequences from *Bothrops diporus* with higher similarity to the analyzed samples. The columns Difference show the differences in KDa between the calculated mass of the sequences and the peaks deconvoluted from the intact mass analysis.

ID	Monoisotopic mass (KDa)	Molecular mass (KDa)	Molecular formula	Difference to PEAK A (KDa)	Difference to PEAK B (KDa)	Difference to PEAK C (KDa)
AFJ79207	13,655.9032	13,665.12		73.588	-12.427	-144,166
AFJ79208	13,625.9039	13,635.09	C ₅₈₆ H ₈₇₀ N ₁₅₈ O ₁₉₁ S ₁₅ C ₅₈₄ H ₈₆₈ N ₁₆₀ O ₁₈₉ S ₁₅	43.558	-42.457	-174,196

simulation, indicating the dynamic nature of the substrate within the enzyme's active site. Moreover, in Panel E, critical catalytic residues within the enzyme, including Asp49, His48, and Tyr52, exhibited significant interactions with DLPC, reinforcing their role in stabilizing the substrate within the binding pocket.

3.3. In vitro assays with HUVECs

BmPLA₂-A at concentrations 3.125, 6.25, 12.5, 25, and 50 µg/mL did not have any effect on HUVECs cell viability at different time intervals (3, 6, and 24 h) evaluated. As presented in Fig. 7, there was no statistical difference between the different concentrations used and the control group (DMEM).

The effect of BmPLA₂-A at different concentrations on the adhesion and detachment of HUVECs cells after 30 min and 1 h of incubation was also evaluated (supplementary material 4 and 5). The BmPLA₂-A, at the concentrations tested (3.125, 6.25, 12.5, 25, and 50 µg/mL), did not impact cell adhesion. Furthermore, no detachment of HUVECs was observed across all concentrations assessed, indicating that BmPLA₂-A does not interfere with these cellular processes under the experimental conditions employed.

In Fig. 8, the impact of BmPLA₂-A (50 µg/mL) on HUVECs was assessed. In the control group (Panel A), cells cultured in DMEM exhibited well-organized and evenly distributed actin filaments (green), with numerous filopodia and intact cell-cell interactions. However, treatment with BmPLA₂-A (Panel B) led to pronounced contraction of actin filaments, disruption of cell-cell interactions, and a marked reduction in the number of filopodia. This reduction was quantified in Panel C, showing a significant decrease in filopodia per cell compared to the control. Panel D further demonstrates a substantial decrease in cell area following 1 h of incubation with BmPLA₂-A, reflecting cell contraction and morphological remodeling. Additionally, Panel E reveals an increased fluorescence intensity near the cortical actin in BmPLA₂-A-treated cells, possibly indicating actin stress fiber formation and remodeling. Together, these results suggest that BmPLA₂-A induces cytoskeletal reorganization, leading to changes in cell shape and impaired cell-cell interactions.

The supernatant from the incubation of BmPLA₂-A with HUVECs was utilized for cytokine quantification. IL-1β production was evaluated after 3 and 6 h, and no release of this mediator was detected at the evaluated time points. In contrast, IL-6 and IL-8 release was observed across all evaluated time intervals and conditions, including the control group (Fig. 9 and supplementary material 6–7), though no significant increase in their release was noted. Therefore, it can be concluded that BmPLA₂-A did not induce the release of these cytokines by HUVECs, indicating that the detected levels represent their expression. Regarding

the release of TNF by HUVEC cells, it was observed that BmPLA₂-A also did not induce the release of this cytokine when exposed to different concentrations (Fig. 9). TNF release occurred only in the presence of PMA (positive control) significantly compared to the negative control (DMEM).

4. Discussion

The first complete biochemical characterization of an acidic PLA₂ from the venom of *B. mattogrossensis*, here named BmPLA₂-A, is reported. Other PLA₂s have also been purified using simplified procedures based on CM-Sepharose and/or reverse phase, such as those, PLA₂s from *Bothrops moojeni* [35–37], *B. pirajai* [38,39], *B. jararacussu* [40,41], *B. alternatus* [42,43] and *B. mattogrossensis* [44]. In this study, we employed three chromatographic steps to isolate BmPLA₂-A, as previously described by Furtado et al., (2014) [45], who isolated an acidic phospholipase from *B. atrox* venom using CM-Sepharose, butyl-Sepharose, and reverse phase chromatography.

Numerous studies have been conducted to investigate the mechanism of action of snake PLA₂s in different cells and organs; however, research on phospholipases from *Bothrops mattogrossensis* remains limited. It is crucial to underscore the presence of two seminal studies in the literature that provide in-depth insights into PLA₂s from *B. mattogrossensis*. The first, conducted by Moura et al., (2014) [44], focused on the purification and characterization of three basic PLA₂s named BmatTX-I, II, and III. The second, by Alfonso et al. (2019) [46], isolated and characterized a basic PLA₂, BmatTX-IV.

The isolated BmPLA₂-A exhibited a molecular mass of approximately 15 kDa as determined by SDS-PAGE and was identified as an acidic enzyme with a theoretical pI of 4.91 (Table 2). Acidic PLA₂s from snake venoms typically have molecular masses ranging from 13 to 16 kDa [40,47,48] and pI values between 4.0 and 5.5. Some examples of it include BthA-I-PLA₂ with 13.7 kDa and pI 4.5, BpirPLA₂-I with 13.7 kDa and pI 4.8, Bp-PLA₂ with 15.8 kDa and pI 4.3, BpPLA₂-TXI with 13.6 kDa and pI 4.9, BmooPLA₂ with 13.6 kDa and pI 5.2, and BI-PLA₂ with 15 kDa and pI 5.4 [39,41,49–52].

We also assessed the phospholipase activity of BmPLA₂-A, confirming that its catalytic activity surpassed that of the well-characterized BthTX-II (Fig. 1) [33]. This catalytic activity was corroborated by the results of LC-MS/MS, indicating the presence of an aspartic acid (D) at position 49 (Fig. 3). Notably, to date, all acidic PLA₂s purified from Viperidae venoms present an Asp residue at position 49 [39,53].

The acidic residue Asp49 was consistently identified across all digestions, supported by high-quality MS² spectra (supplementary material 3). The consensus sequences proposed by de novo protein assembly with Stitch suggested 2 aminoacidic exchanges in the C-terminus of the

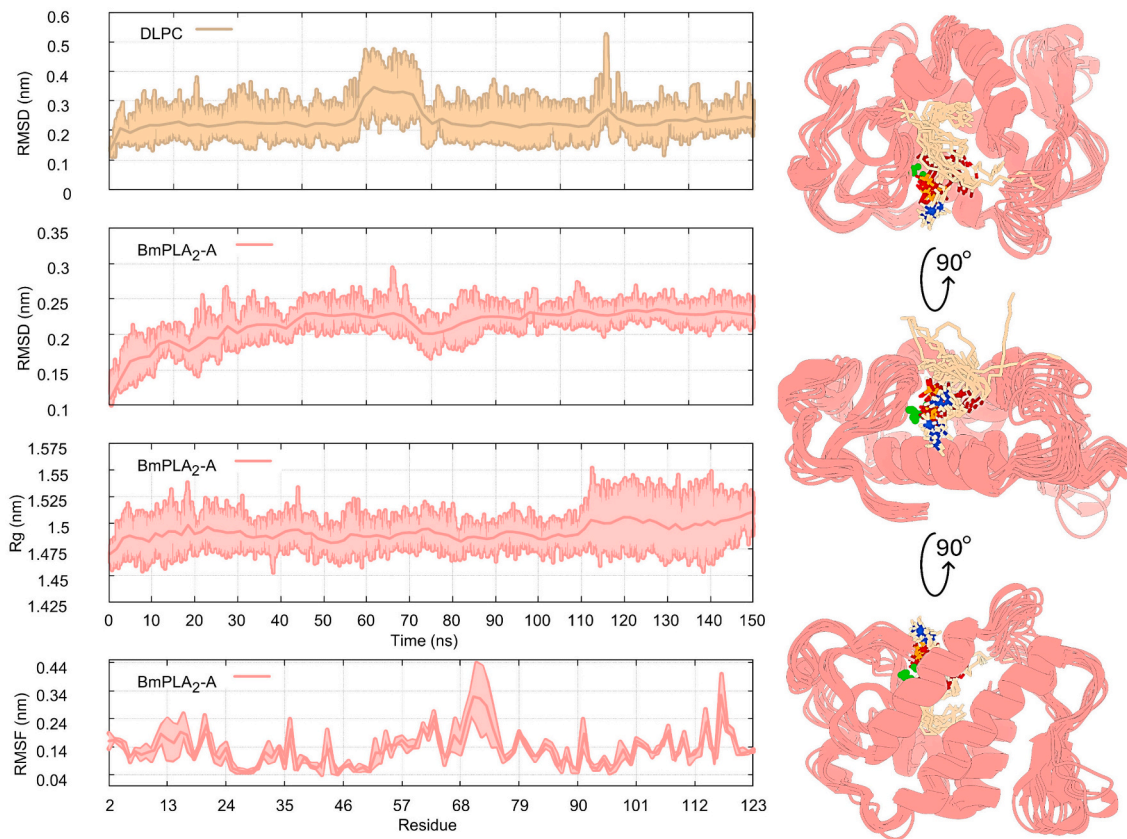


Fig. 5. Contact analysis of the BmPLA₂-A + DLPC + Ca²⁺ complex over 300 ns of simulation. (A) Structural representation of BmPLA₂-A bound to Ca²⁺ and DLPC, highlighting fundamental interactions with Ca²⁺ and catalytic residues. (B) A detailed view of DLPC shows atom positioning and numbering. (C) Mean interaction scores between Ca²⁺ and DLPC atoms. (D) SASA of DLPC over time, reflecting substrate dynamics in the active site. (E) Mean interaction scores between BmPLA₂-A residues and DLPC, underscoring key stabilization points for catalysis.

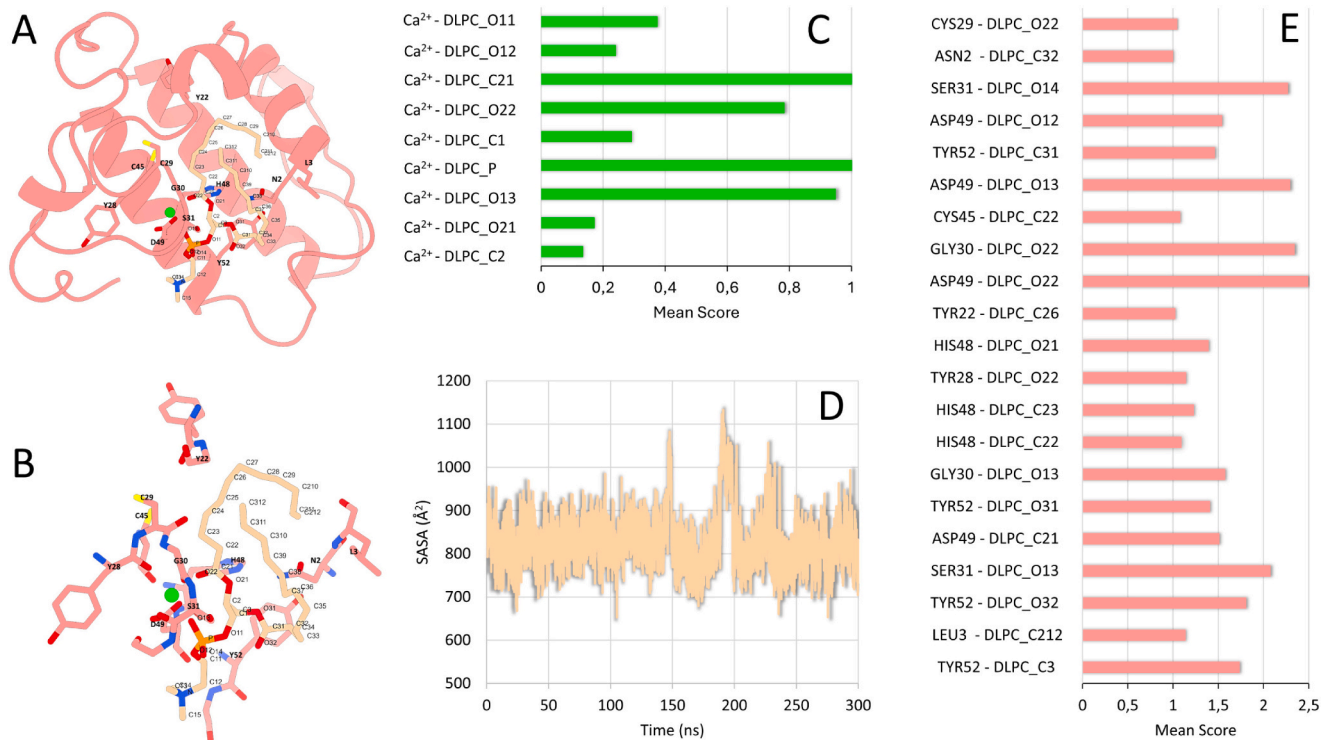


Fig. 6. Cell viability assay (MTT) with HUVECs after incubation at different time intervals (3, 6, and 24 h). DMEM (negative control) and different concentrations of BmPLA₂-A (3.125, 6.25, 12.5, 25, and 50 µg.mL⁻¹) were used.

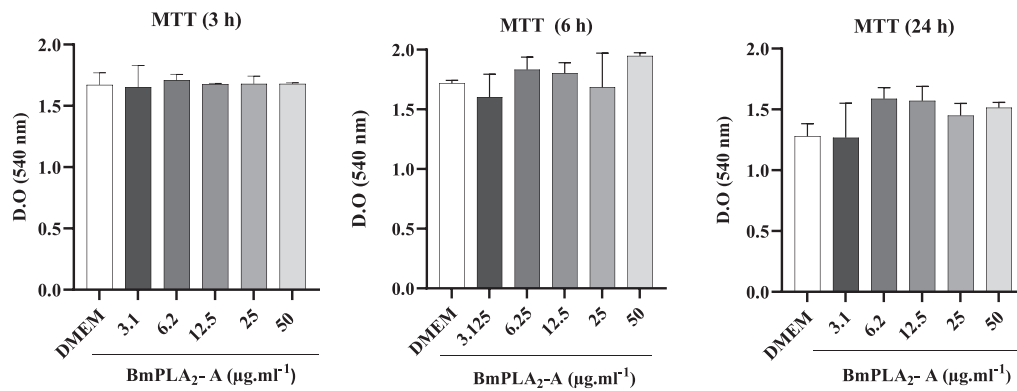


Fig. 7. Immunofluorescence microscopy assay. (A) HUVECs incubated with DMEM. (B) HUVECs incubated for 1 h with 50 µg.mL⁻¹ of BmPLA₂-A. (C) Number of filopodia per cell in the control (DMEM) and BmPLA₂-A groups. (D) Area per cell in the control (DMEM) and BmPLA₂-A groups. (E) Fluorescence intensity in the control (DMEM) and BmPLA₂-A groups. Statistical significance is indicated by an asterisk (*).

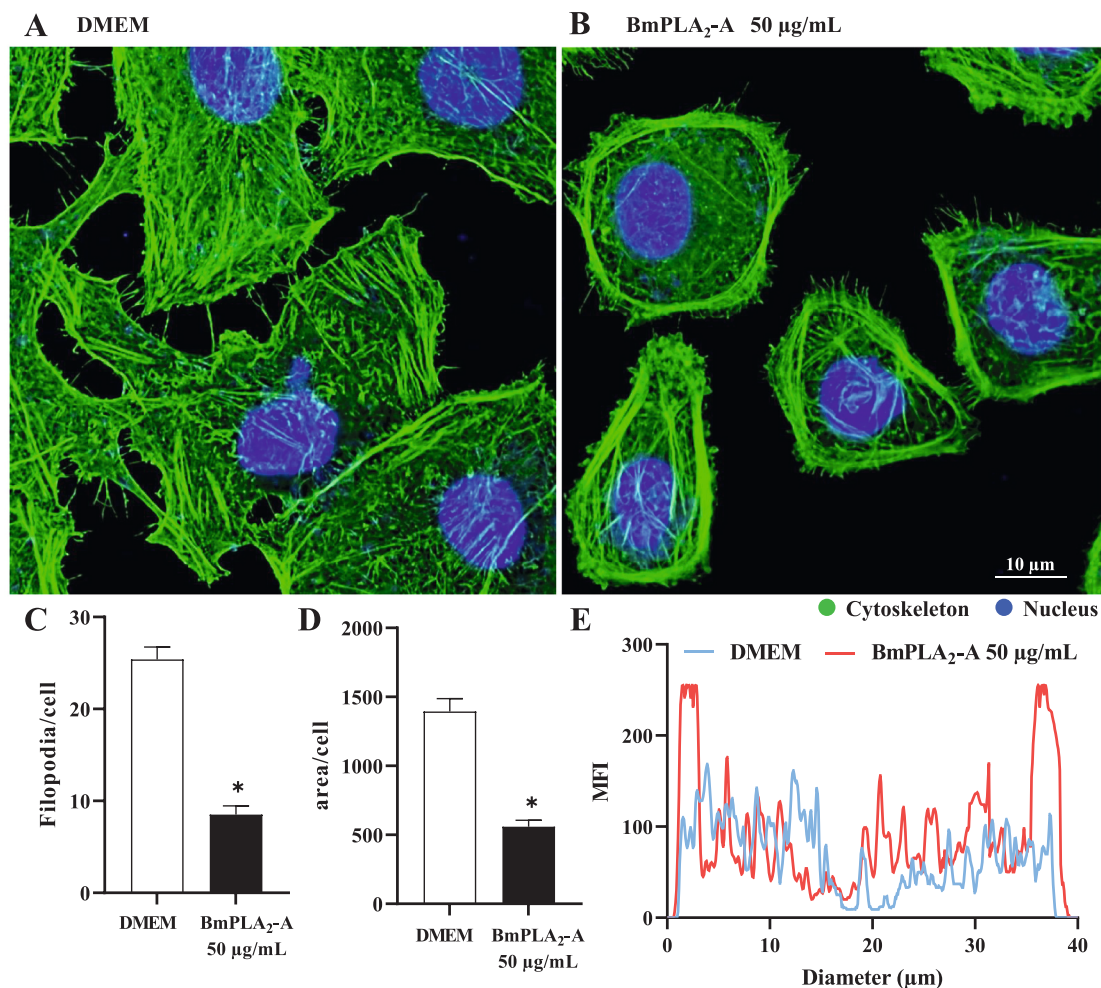


Fig. 8. Cytokine release assays using HUVECs (human umbilical vein endothelial cells) incubated with various concentrations of BmPLA₂-A (3.125, 6.25, 12.5, 25, and 50 µg/mL) for 3 and 6 h. Negative (DMEM) and positive controls (LPS and PMA) were included. The production of IL-6 (A), IL-8 (B), and TNF-α (C) was measured. Statistical significance is indicated by an asterisk (*).

protein PC to QD. However, when these sequences were used as the database for PSM in PEAKS, these exchanges could not be confirmed, therefore it is more likely that, in BmPLA₂, the C-terminus is PC.

The mass differences between the peaks observed in the intact mass analysis may be attributed to aminoacidic exchanges or post-translational modifications (Fig. 2). Peptide sequencing was conducted

considering *N*-acetylation (+42 Da), Met oxidation (+15,99 Da), and Asn deamidation (+0,98 Da) as possible modifications. From the total of 8212 features sequenced by peptide mapping, 2692 displayed a modification, indicating the presence of PTM in the analyzed sample. However, the data here gathered is insufficient to confidently ascertain which specific PTM's are present in the intact sample, or whether the

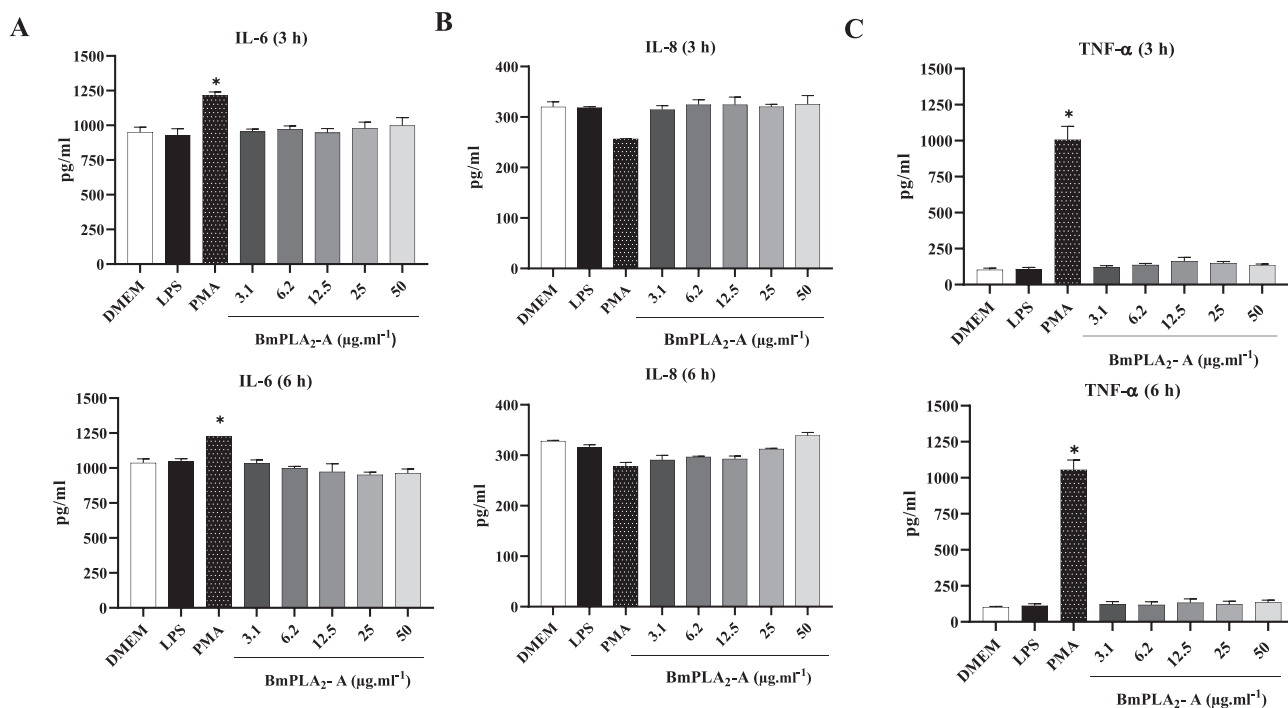


Fig. 9. Sequence alignment of AFJ79207.1 and AFJ79208.1 acidic secretory phospholipases A₂ (sPLA₂-II) from *Bothrops diporus* venom. Identical residues are highlighted in blue, with conservation, quality, and consensus scores shown below. The sequences differ by only four amino acids, with 100 % coverage confirmed by peptide mapping and de novo sequencing. (For interpretation of the references to colour in this figure legend, the reader is referred to the web version of this article.)

mass difference between Peaks A and B is indeed due to PTM (Fig. 2).

PEAKS Spider was employed to search for potential aminoacidic exchanges within the proposed sequences; however, no mutation site with high confidence score was found (data not shown). This does not exclude the possibility of different sequences being present in the sample. Further analysis, including genomic or transcriptomic of *Bothrops matogrosensis* could provide confirmation of the sequence.

The structural analysis of extracellular PLA₂ enzymes across various species has revealed a remarkable degree of similarity, particularly in residues essential for catalytic activity. Consistent with previous findings by Castro-Amorim et al. (2023) [54], the catalytic residues within the active site, such as His48, Asp49, and Tyr52, remain highly conserved among the resolved structures. This study's multiple sequence alignment (MSA) of PLA₂ enzymes from different snake species confirmed the conservation of these critical functional residues, especially those involved in catalysis and calcium binding. Furthermore, the retention of cysteine residues, essential for forming disulfide bridges, underscores the structural stability of the enzyme across species, aligning with earlier reports on PLA₂ stability [54]. The alignment also revealed some sequence variability in regions unrelated to catalysis, potentially reflecting to species-specific functional adaptations. These differences may contribute to variations in venom toxicity and target specificity, suggesting that evolutionary pressures have driven diversification in venom composition while maintaining core enzymatic functions [55].

The catalytic mechanism underlying PLA₂-mediated phospholipid hydrolysis involves the nucleophilic attack at the sn-2 ester bond of the substrate. This process leads to the formation of a tetrahedral intermediate, stabilized by a calcium ion coordinated by Asp49, along with the backbone oxygen atoms of Gly30, Trp28, and Gly35 within the protein structure. His48 functions as the nucleophile during ester hydrolysis, in a manner analogous to the active center serine in esterases. Upon attacking the substrate carbonyl carbon, a nearby water molecule prompts the imidazole ring of His48 to accept a proton, thereby facilitating the reaction [54].

The PLA₂ substrate, DLPC, is characterized by its elongated, amphipathic structure, with a polar head group oriented opposite to the two parallel non-polar acyl chains. X-ray crystallography of several native PLA₂s has elucidated the enzyme's active site, revealing a polar region surrounding the active site calcium and a less polar region adjacent to Leu2 [56]. The amphipathic properties of both the active site and the substrate, combined with the known cleavage of the sn-2 ester bond, delineate the general binding mode of DLPC to PLA₂.

Building on this understanding, the molecular docking predictions revealed a high-affinity bound conformation for DLPC into the BmPLA₂-A active site (Fig. 6). In this binding orientation, the DLPC sn-2 ester bond is positioned near the active site His48, reflecting the most likely native interaction between enzyme and substrate. This robust interaction suggests a high substrate specificity of BmPLA₂-A, critical for its enzymatic function. This conclusion is further supported by enzymatic assays using 4N3OBA, where BmPLA₂-A exhibited superior catalytic efficiency compared to BthTX-II (Fig. 1).

Limited MD simulation studies of catalytically active PLA₂ reported in the literature have sought to explore the conformational dynamics associated with enzyme activity. Additionally, noteworthy that many of these studies were performed either in a vacuum or with considerably short simulation durations, restricting their effectiveness in capturing slow conformational rearrangements [57].

To achieve a more thorough understanding of BmPLA₂-A's enhanced catalytic activity, the MD simulations conducted herein were conducted in a solvated environment, extending the simulation duration and replicating optimal conditions for the enzymatic activity. This approach enables a more precise depiction of the enzyme's behavior, offering valuable insights into the mechanistic foundations that drive its catalytic efficiency.

Based on the RMSD variations observed over 150 ns of MD simulations and the Rg of the overall three-dimensional structure, the binding mode with the DLPC substrate has minimal impact on the structure of BmPLA₂-A. Essential secondary structures, such as alpha-helices and beta-sheets, remained unchanged throughout the simulations,

demonstrating that the enzyme retained its native structural integrity in the presence of its substrate, reflecting the simulation's robustness.

Moreover, the fluctuations observed in DLPC RMSD demonstrate the substrate's dynamic behavior within the active site cleft, especially regarding conformational changes and the flexibility of the sn-1 acyl chain and the head group. The sn-1 acyl chain undergoes extension, adopting a conformation increasingly similar to that observed in crystallographic studies of phospholipids [58].

An intriguing aspect of these enzymes concerns the physiological configuration of the active site in the presence of Ca^{2+} . Most structures of catalytically active PLA_2 in the Protein Data Bank lack a bound calcium ion in their resolved crystallographic models. When present, these ions are typically at concentrations significantly higher than physiological levels [57]. Additionally, prior research indicates the presence of other ions, such as Na^+ , substituting for calcium in the protein-binding loop. Although some crystallographic structures in the PDB do reveal the presence of calcium ions within the calcium-binding loop, kinetic data suggest a low calcium affinity for this binding site, with a dissociation constant of $100 \mu\text{M}$ [59].

Thus, previous studies employing MD simulations, whether in vacuum or aqueous environments, often had to apply positional restraint forces on the calcium ion [60] to investigate the catalytic mechanism of PLA_2 . Despite these efforts, such simulations revealed that none of the conditions employed could maintain the cation at its binding loop for more than five nanoseconds [56,61].

This phenomenon may be partially attributed to the interfacial activation of PLA_2 , where the stability of the calcium ion at the active site is influenced by the phospholipase's proximity to or penetration into the lipid bilayer more apolar environment. Indeed, the hydrolytic activity of sv PLA_2 on phospholipids increases significantly and abruptly (up to 10,000-fold) when monomeric phospholipids aggregate to form micelles at their critical micellar concentration [62].

The clustering analysis of the MD trajectories revealed that Bm PLA_2 -A adopts multiple stable conformations when bound to DLPC and Ca^{2+} . These conformations represent critical states the enzyme might occupy during its catalytic cycle. Most importantly, the coordination shell of Ca^{2+} was essentially maintained during the 150 ns MD simulation replicas, which amounts to 300 ns of simulations with the calcium conserved within its binding site.

The RMSF analysis of the Bm PLA_2 -A + DLPC + Ca^{2+} complex provides valuable insights into the enzyme's structural flexibility and substrate interaction dynamics, delineating distinct regions of heightened flexibility and relative rigidity throughout the protein. Consistent with observations from prior molecular dynamics studies [57,61,63], residues 70–73 at the loop region exhibited the most pronounced fluctuations, suggesting their involvement in the enzyme's dynamic adjustment rather than directly contributing to the stable association with DLPC. These residues likely function as hinge points, facilitating conformational changes that enhance substrate binding during interfacial activation and might promote optimal positioning for efficient catalysis [64].

The contact analysis highlights the pivotal role of Ca^{2+} in stabilizing DLPC, with robust and consistent interactions observed between Ca^{2+} and fundamental DLPC atoms, including P, O13, O22, and C21. These interactions ensure precise alignment and stabilization of the substrate, a prerequisite for efficient catalytic activity [60,61,65]. This observation is consistent with the well-characterized role of Ca^{2+} in Asp49- PLA_2 enzymes, where the ion not only facilitates substrate binding but also lowers the activation energy required for the transition state during hydrolysis [54].

The contact analysis (Fig. 6E) further revealed significant interactions between vital catalytic residues, including Asp49, His48, Tyr52, and the DLPC substrate [55]. These residues engage with the substrate in a highly coordinated manner, as evidenced by their low RMSF values, reflecting the stability of the catalytic core. Specifically, Asp49 is pivotal in ensuring the precise coordination of Ca^{2+} and

facilitating the nucleophilic attack on the sn-2 ester bond [54,66]. This stable core, in contrast to the more flexible regions of the enzyme, supports the dynamic adjustments required for substrate binding and catalytic turnover [57]. The low RMSF values in the active site region align with the contact analysis, indicating a stable interaction network that underscores the necessity of a rigid catalytic environment for efficient hydrolysis.

The fluctuations in solvent-accessible surface area (SASA) observed in the DLPC substrate (Fig. 6D) provide further evidence of the substrate's dynamic behavior within the enzyme's active site, underscoring the critical role of flexibility in substrate handling. These fluctuations likely correspond to the enzyme's interfacial activation mechanism [57], where substrate regions periodically become exposed to the solvent, potentially facilitating catalytic turnover. The dynamic repositioning of the substrate within the active site indicates conformational changes that occur at the lipid-water interface, a characteristic feature of interfacial activation [67]. These structural adjustments enhance the enzyme's catalytic efficiency, allowing for optimal substrate alignment during hydrolysis process [57].

These findings highlight the crucial role of Ca^{2+} mediated stabilization and fundamental residue interactions in ensuring substrate alignment and promoting efficient catalysis. They further emphasize the finely tuned balance of flexibility and rigidity essential for the functional activity of Asp49- PLA_2 . The successful simulation of the native Bm PLA_2 -A + Ca^{2+} -DLPC complex offers valuable insights into the enzyme's hydrolytic behavior in aqueous environments. It presents a promising model for developing novel strategies to target PLA_2 in disease treatment. Additionally, these simulations may inform the design of specific inhibitors to modulate PLA_2 activity with potential therapeutic applications.

Snake venom PLA_2 s play a pivotal role in the initiation of inflammatory processes [9,68]. Interactions between circulating leukocytes and the vascular endothelium represent not only a crucial event in immune surveillance and defense but are also critically implicated in the pathogenesis of various inflammatory and immune disorders. Endothelial cell adhesion is an important event for cell migration, tissue repair, angiogenesis, and vascular integrity maintenance. Therefore, adhesion is a dynamic and cyclic event within endothelial cell migration because the latter depends on cellular morphological polarization; extension of the plasma membrane toward the movement; adhesion of the fore-polarized site; cell contraction, and detachment of the hind-polarized site [69].

In the present study, we evaluated the effects of Bm PLA_2 -A on HUVECs. Bm PLA_2 -A did not impact HUVEC viability, indicating low toxicity to this cell type (Fig. 7). There are limited reports in the literature regarding the effects of venoms and/or isolated toxins on endothelial cell physiology. Díaz et al. (2005) [70] demonstrated that BaP1, a P-I SVMP present in *B. asper* snake venom, did not exhibit cytotoxicity toward human vascular endothelial cells (EA.hy926) at comparable concentrations. Aché et al. (2015) [71] working with a BpMP-II, from *B. pauloensis* venom, showed that the toxin reduced the viability of the murine endothelial cell line (tEnd) at concentrations exceeding $20 \mu\text{g}/\text{mL}$. Similarly, Santana et al. (2024) [30] showed that BjussuMP-II exhibited no toxicity to HUVEC at any concentration tested.

In line with these findings, Cedro et al. (2018) [72] also demonstrated that BJ- PLA_2 -I exhibited low cytotoxic effects in PBMCs. This reduced cytotoxicity has also been reported for other acidic PLA_2 s. For instance, De Albuquerque Modesto et al. (2006) [73] demonstrated that BE-I- PLA_2 , an acidic PLA_2 from *B. erythromelas* venom, showed no toxic effects on HUVEC. Similarly, Nunes et al. (2011) [74] observed low cytotoxicity of BI- PLA_2 from *B. leucurus* venom in PBMC. Conversely, certain acidic PLA_2 s have demonstrated considerable cytotoxicity against tumor cell lines. Roberto et al. (2004) [75] reported that BthA-I- PLA_2 from *B. jararacussu* venom significantly reduced the viability of Jurkat and SK-BR-3 cells, while BmooTX-I from *B. moojeni* venom [76] and MTX-I from *B. brazili* venom [77] also displayed strong cytotoxic

effects on Jurkat cells. These contrasting responses underscore the complex nature of PLA₂ activities, suggesting that their biochemical properties play a critical role in determining their specific effects on both normal and tumor cells.

Despite BmPLA₂-A's non-toxic nature toward endothelial cells, studies have shown that *Bothrops* venoms can induce endothelial cell detachment and loss of adhesion capacity [78–81]. Interestingly, BmPLA₂-A, at concentrations ranging from 3 to 50 µg/mL, did not induce HUVECs detachment after 1 h of incubation and did not interfere in adhesion (supplementary material 4 and 5), suggesting a potential role in affecting the expression of adhesion molecules of the cell membrane without affecting cell viability. Moreover, morphological modifications in HUVECs specifically in actin filaments, were observed, including a reduction in the number of filopodia in the presence of the BmPLA₂-A (Fig. 8). In a study conducted by Dos Santos et al. (2020) [82], the authors demonstrated that HUVECs, when incubated with *Alternanthera*-C, exhibited morphological alterations, including cytoskeletal disorganization and a reduced number of filopodia, similar to the effects observed when incubated with BmPLA₂-A. It is well established that changes in the cellular environment can lead to alterations in cell morphology [83], and cells can adapt their morphology in different environments through modifications in their actin cytoskeletons [84]. Nevertheless, further studies are required to elucidate the mechanism of action of BmPLA₂-A and the specific pathways to induce these morphological changes in HUVECs.

Next, we investigated whether BmPLA₂-A affects cytokines production in HUVEC cells. Across all concentrations studied (3–50 µg/mL), BmPLA₂-A did not induce cytokine production in HUVEC cells (Fig. 9 and supplementary material 6–7). Our data align with those of Andrade et al. (2019) [85], who evaluated the effects of different concentrations of crotoxin (25–200 µg/mL) on endothelial cells and similarly observed no release of IL-6, IL-8, or IL-1β by HUVECs.

Furthermore, TNF-α, a proinflammatory cytokine, plays a crucial role in regulating acute inflammation and leukocyte activation. Patients bitten by Viperidae snakes may experience exacerbated conditions due to TNF-α production by endothelial cells in response to proinflammatory cytokines like IL-1β [86]. However, our results indicate that BmPLA₂-A did not induce TNF-α release in HUVEC cells, in contrast to the significant increase observed with PMA stimulation (Fig. 9). These findings are consistent with those of Santana et al. (2024) [30], where BjussuMP-II also did not induce TNF-α release.

The differential effects of BmPLA₂-A from *Bothrops mattogrossensis* on endothelial cells likely attributable to its acidic nature and structural features. Although BmPLA₂-A shares catalytic similarities with other snake venom PLA₂s, its impact on endothelial cells appears less aggressive, suggesting a distinct, milder mechanism of action. The absence of pro-inflammatory cytokine production, such as TNF-α, further emphasizes its subtle effects compared to more inflammatory PLA₂s within the *Bothrops* genus. Sequence analysis reveals that BmPLA₂-A lacks the highly cationic and hydrophobic C-terminal region (115–129) found in *Bothrops asper* myotoxin II [87], which is known to be crucial for cytotoxicity. This structural difference likely prevents interactions with cellular targets, such as membranes, thereby explaining the observed lack of cytotoxicity [87]. These findings underscore the need for further comparative studies to unravel the molecular determinants of these differential effects.

This study contributes significantly to the current knowledge of acidic PLA₂s, particularly from *Bothrops mattogrossensis* venom, which remains underexplored. The structural and functional attributes of BmPLA₂-A emphasizing the diverse roles of PLA₂s in venom physiology and their potential biomedical applications. These findings underscore the enzyme's relevance not only for unraveling the biochemical mechanisms underlying envenomation but also for informing therapeutic strategies targeting inflammatory and infectious diseases.

5. Conclusion

In conclusion, this study addressed the existing knowledge gap regarding the characterization of acidic PLA₂ from *B. mattogrossensis* venom. Through the use of chromatographic techniques followed by comprehensive biochemical and biological analyses, we isolated, characterized, and assessed the activity of BmPLA₂-A. Our findings demonstrate that BmPLA₂-A exhibits superior catalytic activity compared to BthTX-II and shares significant homology with acidic PLA₂s from other snake species.

Furthermore, our investigation into the effects of BmPLA₂-A on endothelial cells, revealed that this enzyme induces morphological changes and reduces the number of filopodia, without triggering the release of cytokines (IL-6, IL-8, IL-1β, and TNF). These results enhance our understanding of the biochemistry and physiology of *B. mattogrossensis* PLA₂s and provide valuable insights into the impact of acidic PLA₂ on endothelial cells, thereby laying the groundwork for future studies aimed at elucidating these processes in greater detail. Lastly, the extensive computational analysis of the native BmPLA₂-A + Ca²⁺+DLPC complex offers deeper insights into the enzyme's hydrolytic mechanism and serves as a potential model for the development of novel therapeutic strategies targeting PLA₂-mediated pathologies.

CRedit authorship contribution statement

Micaela de Melo Cordeiro Eulálio: Writing – original draft, Validation, Software, Methodology, Formal analysis, Conceptualization. **Anderson Maciel de Lima:** Validation, Software, Methodology, Formal analysis. **Rodrigo Soares Caldeira Brant:** Writing – original draft, Validation, Software, Methodology, Formal analysis, Conceptualization. **Aleff Ferreira Francisco:** Writing – original draft, Validation, Software, Methodology, Formal analysis, Conceptualization. **Hallison Mota Santana:** Methodology, Formal analysis. **Mauro Valentino Paloschi:** Methodology, Formal analysis. **Sulamita da Silva Setúbal:** Methodology, Funding acquisition, Formal analysis. **Carolina Pereira da Silva:** Methodology, Formal analysis. **Milena Daniela Souza Silva:** Methodology, Formal analysis. **Charles Nunes Boeno:** Methodology, Formal analysis. **Anderson Makoto Kayano:** Validation, Software, Methodology, Formal analysis. **Paula Helena Santa Rita:** Methodology. **Leonardo de Azevedo Calderon:** Software, Methodology, Formal analysis. **Andreimar Martins Soares:** Supervision, Funding acquisition, Conceptualization. **Daniela Priscila Marchi Salvador:** Conceptualization. **Juliana Pavan Zuliani:** Writing – original draft, Supervision, Resources, Funding acquisition, Conceptualization.

Funding

The authors extend their gratitude to the Conselho Nacional de Desenvolvimento Científico e Tecnológico (CNPq), Coordenação de Aperfeiçoamento de Pessoal de Nível Superior (CAPES), and Fundação de Amparo à Pesquisa do Estado de Rondônia (FAPERO) for the financial support. The authors thank the Network Technological Platforms from FIOCRUZ for the support and financing of the services provided by Microscopy (RPT-7I), and Bioprospecting and Molecular Interaction (RPT-10B) facilities/FIOCRUZ-Rondonia. This study was supported by grants (428774/2016-4 and 311696/2021-0) from Conselho Nacional de Desenvolvimento Científico e Tecnológico (CNPq). Juliana Pavan Zuliani was a recipient of productivity grant 306672/2014-6 and 311696/2021-0 from Conselho Nacional de Desenvolvimento Científico e Tecnológico (CNPq) and Micaela de Melo Cordeiro Eulálio was the beneficiary of CAPES by Doctoral fellowship.

Declaration of competing interest

The authors declare that they have no known competing financial interests or personal relationships that could have appeared to influence

the work reported in this paper.

Appendix A. Supplementary data

Supplementary data to this article can be found online at <https://doi.org/10.1016/j.ijbiomac.2024.139217>.

Data availability

Data will be made available on request.

References

- [1] C Fernández .E.A., P. Youssef, Snakebites in the Americas: a neglected problem in public health, *Curr. Trop. Med. Rep.* 11 (2024) 19–27, <https://doi.org/10.1007/s40475-023-00309-5>.
- [2] A. Kasturiratne, A.R. Wickremasinghe, N. Silva, N.K. Gunawardena, A. Pathmeswaran, R. Premaratna, L. Savioli, D.G. Lalloo, H.J. de Silva, The global burden of snakebite: A literature analysis and modelling based on regional estimates of envenoming and deaths, *PLoS Med.* 5 (2008) 218, <https://doi.org/10.1371/journal.pmed.0050218>.
- [3] J.P. Chippaux, Snake-bites: appraisal of the global situation, *Bull. World Health Organ.* 76 (1998) 515–524.
- [4] J. Gutiérrez, J. Calvete, A. Habib, et al., Snakebite envenoming, *Nat. Rev. Dis. Primers.* 3 (2017), <https://doi.org/10.1038/nrdp.2017.63>.
- [5] J.A. Campbell, W. Lamar, *The Venomous Reptiles of Latin America*, Cornell University Press, Ithaca, 1989.
- [6] G.P. Fernández, A. Segura, M. Herrera, W. Velasco, G. Solano, J.M. Gutiérrez, G. León, Neutralization of *Bothrops mattogrossensis* snake venom from Bolivia: experimental evaluation of llama and donkey antivenoms produced by caprylic acid precipitation, *Toxicon* 55 (2010), <https://doi.org/10.1016/j.toxicon.2009.07.031>.
- [7] P.E. Bickler, Amplification of snake venom toxicity by endogenous signaling pathways, *Toxins (Basel)* 12 (2) (2020) 68, <https://doi.org/10.3390/toxins12020068>.
- [8] C.C.N. Mamede, B.B. de Sousa Simamoto, D.F. da Cunha Pereira, J. de Oliveira Costa, M.S.M. Ribeiro, F. de Oliveira, Edema, hyperalgesia and myonecrosis induced by Brazilian bothropic venoms: overview of the last decade, *Toxicon* 187 (2020) 10–18, <https://doi.org/10.1016/j.toxicon.2020.08.016>.
- [9] J.P. Zuliani, R.D. Souza, S.S. Setúbal, C.N. Boeno, J.A. Lopes, S.R. Zamuner, Inflammatory effects of phospholipase A₂s present in snake venom of the genus *Bothrops*, in: *SAJAL CHAKRABORTI. (Org.). PHOSPHOLIPASES IN PHYSIOLOGY AND PATHOLOGY: Volume 4: Role of Phospholipases in Inflammation, Gene Expression, and Apoptosis*, 1ed. vol. v. 4, Academic Press from Elsevier, 2023, pp. 173–196.
- [10] J. Castro-Amorim, A. Novo de Oliveira, S.L. Da Silva, A.M. Soares, A.K. Mukherjee, M.J. Ramos, P.A. Fernandes, Catalytically active Snake venom PLA₂ enzymes: an overview of its elusive mechanisms of reaction, *J. Med. Chem.* 27 (2023) 5364–5376, <https://doi.org/10.1021/acs.jmedchem.3c00097>.
- [11] U.K. Laemmli, Cleavage of structural proteins during the assembly of the head of bacteriophage T4, *Nature* 227 (1970) 680–685, <https://doi.org/10.1038/227680a0> (PMID: 5432063).
- [12] C.J. Sobrinho, A.M. Kayano, R. Simões-Silva, J.J. Alfonso, A.F. Gomez, M.C. V. Gomez, F.B. Zanchi, L.A. Moura, V.R. Souza, A.L. Fuly, E. Oliveira, S.L. Silva, J. R. Almeida, J.P. Zuliani, A.M. Soares, Anti-platelet aggregation activity of two novel acidic Asp49-phospholipases A₂ from *Bothrops brazili* snake venom, *Int. J. Biol. Macromol.* 107 (2018) 1014–1022, <https://doi.org/10.1016/j.ijbiomac.2017.09.069>.
- [13] N. Petrovic, C. Grove, P.E. Langton, N.L. Misso, P.J. Thompson, A simple assay for a human serum phospholipase A₂ that is associated with high-density lipoproteins, *J. Lipid Res.* 42 (2001) 1706–1713, [https://doi.org/10.1016/S0022-2275\(20\)32226-4](https://doi.org/10.1016/S0022-2275(20)32226-4).
- [14] E. Gasteiger, C. Hoogland, A. Gattiker, S. Duvaud, M.R. Wilkins, R.D. Appel, A. Bairoch, Protein identification and analysis tools on the ExPASy server, in: J. M. Walker (Ed.), *The Proteomics Protocols Handbook*, Humana Press, New York, 2005, pp. 571–607, <https://doi.org/10.1385/1-59259-890-0:571>.
- [15] D. Schulte, W. Peng, J. Snijder, Template-based assembly of proteomic short reads for De Novo antibody sequencing and repertoire profiling, *Anal. Chem.* 94 (2022) 3961–3969, <https://doi.org/10.1021/acs.analchem.2c01300>.
- [16] M.T. Marty, A.J. Baldwin, E.G. Marklund, G.K.A. Hochberg, J.L.P. Benesch, C. V. Robinson, Bayesian deconvolution of mass and ion mobility spectra: from binary interactions to polydisperse ensembles, *Anal. Chem.* 87 (2015) 4370–4376, <https://doi.org/10.1021/acs.analchem.5b00140>.
- [17] J. Eberhardt, D. Santos-Martins, A.F. Tillack, S. Forli, AutoDock Vina 1.2.0: new docking methods, expanded force field, and python bindings, *J. Chem. Inf. Model.* 23 (2021) 3891–3898, <https://doi.org/10.1021/acs.jcim.1c00203>.
- [18] L.C. Xue, J.P. Rodrigues, P.L. Kastiris, A.M. Bonvin, A. Vangone, PRODIGY: a web server for predicting the binding affinity of protein-protein complexes, *Bioinformatics* 1 (2016) 3676–3678, <https://doi.org/10.1093/bioinformatics/btw514>.
- [19] E. Jurrus, D. Engel, K. Star, K. Monson, J. Brandi, L.E. Felberg, D.H. Brookes, L. Wilson, J. Chen, K. Liles, M. Chun, P. Li, D.W. Gohara, T. Dolinsky, R. Konecny, D.R. Koes, J.E. Nielsen, T. Head-Gordon, W. Geng, R. Krasny, G.W. Wei, M.J. Holst, J.A. McCammon, N.A. Baker, Improvements to the APBS biomolecular solvation software suite, *Protein Sci.* 27 (2018) 112–128, <https://doi.org/10.1002/pro.3280> (Epub 2017 Oct 24).
- [20] M.J. Abraham, T. Murtola, R. Schulz, et al., GROMACS: high performance molecular simulations through multi-level parallelism from laptops to supercomputers, *SoftwareX* 1 (2015) 19–25, <https://doi.org/10.1016/j.softx.2015.06.001>.
- [21] J. Huang, S. Rauscher, G. Nawrocki, T. Ran, M. Feig, B.L. de Groot, H. Grubmüller, A.D. MacKerell, CHARMM36m: an improved force field for folded and intrinsically disordered proteins, *Nat. Methods* 14 (2017) 71–73, <https://doi.org/10.1038/nmeth.4067>.
- [22] X. Daura, K. Gademann, B. Jaun, D. Seebach, W.F. Van Gunsteren, A.E. Mark, Peptide folding: when simulation meets experiment, *Angew. Chem. Int. Ed.* 38 (1999) 236–240, [https://doi.org/10.1002/\(sici\)1521-3773\(19990115\)38:1/2<236::aid-anie236>3.0.co;2-m](https://doi.org/10.1002/(sici)1521-3773(19990115)38:1/2<236::aid-anie236>3.0.co;2-m).
- [23] H.J.C. Berendsen, J.P.M. Postma, W.F. Van Gunsteren, A. DiNola, J.R. Haak, Molecular dynamics with coupling to an external bath, *J. Chem. Phys.* 81 (1984) 3684–3690, <https://doi.org/10.1063/1.448118>.
- [24] W.G. Hoover, Canonical dynamics: equilibrium phase-space distributions, *Phys. Rev. A* 31 (1985) 1695–1697, <https://doi.org/10.1103/PhysRevA.31.1695>.
- [25] M. Parrinello, A. Rahman, Polymorphic transitions in single crystals: a new molecular dynamics method, *J. Appl. Phys.* 52 (1981) 7182–7190, <https://doi.org/10.1063/1.328693>.
- [26] J. Shao, S.W. Tanner, N. Thompson, T.E. Cheatham, III clustering molecular dynamics trajectories: 1. Characterizing the performance of different clustering algorithms, *J. Chem. Theory Comput.* 3 (2007) 2312–2334, <https://doi.org/10.1021/ct700119m>.
- [27] M. Scheurer, P. Rodenkirch, M. Siggel, R.C. Bernardi, K. Schulten, E. Tajkhorshid, T. Rudack, PyContact: rapid, customizable, and visual analysis of noncovalent interactions in MD simulations, *Biophys. J.* 114 (2018) 577–583, <https://doi.org/10.1016/j.bpj.2017.12.003>.
- [28] R.A. Laskowski, M.B. Swindells, LigPlot+: multiple ligand-protein interaction diagrams for drug discovery, *J. Chem. Inf. Model.* 51 (2011) 2778–2786, <https://doi.org/10.1021/ci200227u>.
- [29] E.F. Pettersen, T.D. Goddard, C.C. Huang, E.C. Meng, G.S. Couch, T.I. Croll, et al., UCSF ChimeraX: structure visualization for researchers, educators, and developers, *Protein Sci.* 30 (2021) 70–82, <https://doi.org/10.1002/pro.3943>.
- [30] H.M. Santana, Y.J. Ikenohuchi, M.D.S. Silva, B.J.C. Farias, S.N. Serrath, C.P. Da Silva, J.G.D.S. Magalhães, L.F. Cruz, D.G. Cardozo, A. Ferreira E Ferreira, V.P. Dos Reis, R. Diniz-Sousa, C.N. Boeno, M.V. Paloschi, A.M. DE Lima, A.M. Soares, S.D. S. Setúbal, J.P. Zuliani, Bjussump-II, a venom metalloproteinase, induces the release and cleavage of pro-inflammatory cytokines and disrupts human umbilical vein endothelial cells, *Chem. Biol. Interact.* 1 (394) (2024) 110986, <https://doi.org/10.1016/j.cbi.2024.110986>.
- [31] S.S. Setúbal, A.S. Pontes, J.L. Furtado, A.M. Kayano, R.G. Stábéli, J.P. Zuliani, Effect of *Bothrops alternatus* snake venom on macrophage phagocytosis and superoxide production: participation of protein kinase C, *The Journal of Venomous Animals and Toxins including Tropical Diseases* 17 (2011) 430–441, <https://doi.org/10.1590/S1678-91992011000400010>.
- [32] M.V. Paloschi, C.N. Boeno, J.A. Lopes, C.A.M. Rego, M.D.S. Silva, H.M. Santana, S. N. Serrath, Y.J. Ikenohuchi, B.J.C. Farias, K.P. Felipin, N.M. Nery, V.P. Dos Reis, C. T. de Lima Lemos, J.R. Evangelista, S. Da Silva Setúbal, A.M. Soares, J.P. Zuliani, Reactive oxygen species-dependent-NLRP3 inflammasome activation in human neutrophils induced by l-amino acid oxidase derived from *Calloselasma rhodostoma* venom, *Life Sci.* 1 (308) (2022) 120962, <https://doi.org/10.1016/j.lfs.2022.120962>.
- [33] C.L. Guimarães, S.H. Andrião-Escarso, L.S. Moreira-Dill, B.M. Carvalho, D. P. Marchi-Salvador, N.A. Santos-Filho, C.A. Fernandes, M.R. Fontes, J.R. Giglio, B. Barraviera, J.P. Zuliani, C.F. Fernandes, L.A. Calderón, R.G. Stábéli, F. Albericio, S.L. Da Silva, A.M. Soares, Alkylation of histidine residues of *Bothrops jararacussu* venom proteins and isolated phospholipases A₂: a biotechnological tool to improve the production of antibodies, *Biomed. Res. Int.* 2014 (2014) 981923, <https://doi.org/10.1155/2014/981923>.
- [34] L. Patiny, A. Borel, ChemCalc: a building block for tomorrow's chemical infrastructure, *J. Chem. Inf. Model.* 53 (2013) 1223–1228, <https://doi.org/10.1021/ci300563h>.
- [35] R.G. Stábéli, S.F. Amui, C.D. Sant'Ana, et al., *Bothrops moojeni* myotoxin-II, a Lys49-phospholipase A₂ homologue: an example of function versatility of snake venom proteins, *Comp. Biochem. Physiol. C* 142 (2006) 371–381, <https://doi.org/10.1016/j.cbpc.2005.11.020>.
- [36] N.A. Santos-Filho, L.B. Silveira, C.Z. Oliveira, et al., A new acidic myotoxic, anti-platelet and prostaglandin I₂ inductor phospholipase A₂ isolated from *Bothrops moojeni* snake venom, *Toxicon* 52 (2008) 908–917, <https://doi.org/10.1016/j.toxicon.2008.08.020>.
- [37] A.M. Soares, S.H. Andrião-Escarso, Y. Angulo, et al., Structural and functional characterization of myotoxin I, a Lys49 phospholipase A₂ homologue from *Bothrops moojeni*(Caissaca) snake venom, *Arch. Biochem. Biophys.* 373 (2000) 7–15, <https://doi.org/10.1006/abbi.1999.1492>.
- [38] A.M. Soares, S.H. Andrião-Escarso, R.K. Bortoleto, et al., Dissociation of enzymatic and pharmacological properties of piratoxins-I and -III, two myotoxic phospholipases A₂ from *Bothrops pirajai* snake venom, *Arch. Biochem. Biophys.* 387 (2001) 188–196, <https://doi.org/10.1016/j.toxicon.2003.11.008>.
- [39] S.S. Teixeira, L.B. Silveira, F.M.N. Da Silva, et al., Molecular characterization of an acidic phospholipase A₂ from *Bothrops pirajai* snake venom: synthetic C-terminal

- peptide identifies its antiplatelet region, *Arch. Toxicol.* 85 (2011) 1219–1233, <https://doi.org/10.1007/s00204-011-0665-6>.
- [40] S.H. Andrião-Escarso, A.M. Soares, V.M. Rodrigues, et al., Myotoxic phospholipases A₂ in *Bothrops* snake venoms: effect of chemical modifications on the enzymatic and pharmacological properties of bothropstoxins from *Bothrops jararacussu*, *Biochimie* 82 (2000) 755–763, [https://doi.org/10.1016/s0300-9084\(00\)01150-0](https://doi.org/10.1016/s0300-9084(00)01150-0).
- [41] S.H. Andrião-Escarso, A.M. Soares, M.R. Fontes, A.L. Fuly, F.M. Corrêa, J.C. Rosa, et al., Structural and functional characterization of an acidic platelet aggregation inhibitor and hypotensive phospholipase A₂ from *Bothrops jararacussu* snake venom, *Biochem. Pharmacol.* 64 (2002) 723–732, [https://doi.org/10.1016/s0006-2952\(02\)01210-8](https://doi.org/10.1016/s0006-2952(02)01210-8).
- [42] S.S. Setubal, A.S. Pontes, J.L. Furtado, et al., Action of two phospholipases A₂ purified from *Bothrops alternatus* snake venom on macrophages, *Biochemistry* 78 (2013) 194–203, <https://doi.org/10.1134/S0006297913020089>.
- [43] M.E.G. Denegri, O.C. Acosta, S. Huancahuire-Vega, et al., Isolation and functional characterization of a new acidic PLA₂ Ba SpII RP4 of the *Bothrops alternatus* snake venom from Argentina, *Toxicon* 56 (2010) 64–74, <https://doi.org/10.1016/j.toxicon.2010.02.031>.
- [44] A.A. De Moura, A.M. Kayano, G.A. Oliveira, S.S. Setúbal, J.G. Ribeiro, N.B. Barros, R. Nicolet, L.A. Moura, A.L. Fuly, A. Nomizo, S.L. Da Silva, C.F. Fernandes, J. P. Zuliani, R.G. Stábili, A.M. Soares, L.A. Calderon, Purification and biochemical characterization of three myotoxins from *Bothrops mattogrossensis* snake venom with toxicity against *Leishmania* and tumor cells, *Biomed. Res. Int.* 2014 (2014) 195356, <https://doi.org/10.1155/2014/195356>.
- [45] J.L. Furtado, G.A. Oliveira, A.S. Pontes, S.S. Setúbal, C.V. Xavier, F. Lacouth-Silva, B.F. Lima, K.D. Zaqueo, A.M. Kayano, L.A. Calderon, R.G. Stábili, A.M. Soares, J. P. Zuliani, Activation of J77A.1 macrophages by three phospholipases A₂ isolated from *Bothrops atrox* snake venom, *Biomed. Res. Int.* 2014 (2014) 683123, <https://doi.org/10.1155/2014/683123>.
- [46] J.J. Alfonso, A.M. Kayano, A.F.G. Garay, R. Simões-Silva, J.C. Sobrinho, S. Vouliotis, A.M. Soares, L.A. Calderon, M.C.V. Gómez, Isolation, biochemical characterization and antiparasitic activity of BmatTX-IV, A basic Lys49-phospholipase A₂ from the venom of *Bothrops mattogrossensis* from Paraguay, *Curr. Top. Med. Chem.* 19 (2019) 2041–2048, <https://doi.org/10.2174/1568026619666190723154756>.
- [47] J.M. Gutierrez, B. Lomonte, Phospholipase A₂ myotoxins from *Bothrops* snake venoms, *Toxicon* 33 (1995) 1405–1424.
- [48] C.L. Ownby, H.S.S. De Araujo, S.P. White, J.E. Fletcher, Lysine 49 phospholipase A₂ proteins, *Toxicon* 37 (1999) 411–445.
- [49] D.C. Nunes, R.S. Rodrigues, M.N. Lucena, C.T. Cologna, A.C. Oliveira, A. Hamaguchi, et al., Isolation and functional characterization of proinflammatory acidic phospholipase A₂ from *Bothrops leucurus* snake venom, *Comp. Biochem. Physiol. C Toxicol. Pharmacol.* 154 (2011) 226–233, <https://doi.org/10.1016/j.cbpc.2011.06.003>.
- [50] L.B. Silveira, D.P. Marchi-Salvador, N.A. Santos-Filho, F.P. Silva Jr., S. Marcussi, A. L. Fuly, et al., Isolation and expression of a hypotensive and anti-platelet acidic phospholipase A₂ from *Bothrops moojeni* snake venom, *J. Pharm. Biomed. Anal.* 73 (2013) 35–43, <https://doi.org/10.1016/j.jpba.2012.04.008>.
- [51] F.B. Ferreira, M.S. Gomes, D.L. De Souza, S.N. Gimenes, L.E. Castanheira, M. H. Borges, R.S. Rodrigues, K.A. Yoneyama, M.I. Brandeburgo, V.M. Rodrigues, Molecular cloning and pharmacological properties of an acidic PLA₂ from *Bothrops pauloensis* snake venom, *Toxins (Basel)* 5 (2013) 2403–2419, <https://doi.org/10.3390/toxins5122403>.
- [52] R.S. Rodrigues, L.F. Izidoro, S.S. Teixeira, L.B. Silveira, A. Hamaguchi, M.I. Homs-Brandeburgo, et al., Isolation and functional characterization of a new myotoxic acidic phospholipase A₂ from *Bothrops pauloensis* snake venom, *Toxicon* 50 (2007) 153–165, <https://doi.org/10.1016/j.toxicon.2007.03.005>.
- [53] J. Fernandez, J.M. Gutiérrez, Y. Angulo, et al., Isolation of an acidic phospholipase A₂ from the venom of the snake *Bothrops asper* of Costa Rica: biochemical and toxicological characterization, *Biochimie* 92 (2010) 273–283, <https://doi.org/10.1016/j.biochi.2009.12.006>.
- [54] J. Castro-Amorim, et al., Catalytically active snake venom PLA₂ enzymes: an overview of its elusive mechanisms of reaction: miniperspective, *J. Med. Chem.* 66 (2023) 5364–5376, <https://doi.org/10.1021/acs.jmedchem.3c00097>.
- [55] A. Oliveira, L. Bleicher, C.G. Schrago, F.P. Silva Junior, Conservation analysis and decomposition of residue correlation networks in the phospholipase A₂ superfamily (PLA₂s): insights into the structure-function relationships of snake venom toxins, *Toxicon* 146 (2018) 50–60, <https://doi.org/10.1016/j.toxicon.2018.03.013>.
- [56] S.T. Jones, P. Ahlström, H.J.C. Berendsen, R.W. Pickersgill, Molecular dynamics simulation of a phospholipase A₂-substrate complex, *Biochim. Biophys. Acta Protein Struct. Mol. Enzymol.* 1162 (1993) 135–142, [https://doi.org/10.1016/0167-4838\(93\)90139-1](https://doi.org/10.1016/0167-4838(93)90139-1).
- [57] T.C. De Oliveira, H.L.N. De Amorim, J.A. Guimarães, Interfacial activation of snake venom phospholipases A₂ (svPLA₂) probed by molecular dynamics simulations, *J. Mol. Struct. (THEOCHEM)* 818 (2007) 31–41, <https://doi.org/10.1016/j.theochem.2007.05.006>.
- [58] H. Hauser, I. Pascher, R.H. Pearson, S. Sundell, Preferred conformation and molecular packing of phosphatidylethanolamine and phosphatidylcholine, *Biochimica et Biophysica Acta (BBA) - Reviews on Biomembranes* 650 (1981) 21–51, [https://doi.org/10.1016/0304-4157\(81\)90007-1](https://doi.org/10.1016/0304-4157(81)90007-1).
- [59] B.-Z. Yu, J. Rogers, G.R. Nicol, K.H. Theopold, K. Seshadri, S. Vishweshwara, M. K. Jain, Catalytic significance of the specificity of divalent cations as K S * and k c at * cofactors for secreted phospholipase A₂, *Biochemistry* 37 (1998) 12576–12587, <https://doi.org/10.1021/bi9728607>.
- [60] H. Ohishi, et al., Molecular dynamics simulation of 1,2-Dilauroyl-L-phosphatidylethanolamine binding to phospholipase A₂: an attempt to explain the selective hydrolysis of substrate fatty acid ester at position 2, *The Journal of Biochemistry* 114 (1993) 210–214, <https://doi.org/10.1093/oxfordjournals.jbchem.a124156>.
- [61] I.A. Emmanuel, et al., The role of calcium on the active site of Snake venom phospholipase A₂: molecular dynamics simulations, *Computational Biology and Bioinformatics* 4 (2016) 10, <https://doi.org/10.11648/j.cbb.20160401.12>.
- [62] P.M. Kilby, W.U. Primrose, G.C.K. Roberts, Changes in the structure of bovine phospholipase A₂ upon micelle binding, *Biochem. J.* 305 (1995) 935–944, <https://doi.org/10.1042/bj3050935>.
- [63] F. Zhou, K. Schulten, Molecular dynamics study of phospholipase A 2 on a membrane surface, *Proteins Struct. Funct. Bioinforma* 25 (1996) 12–27, [https://doi.org/10.1002/\(SICI\)1097-0134\(199605\)25:1<12::AID-PROT2>3.0.CO;2-M](https://doi.org/10.1002/(SICI)1097-0134(199605)25:1<12::AID-PROT2>3.0.CO;2-M).
- [64] L.F. Vieira, A.J. Magro, C.A.H. Fernandes, B.M. De Souza, W.L.G. Cavalcante, M. S. Palma, J.C. Rosa, A.L. Fuly, M.R.M. Fontes, M. Gallacci, D.S. Butzke, L. A. Calderon, R.G. Stábili, J.R. Giglio, A.M. Soares, Biochemical, functional, structural and phylogenetic studies on Interco, a new isoform phospholipase A₂ from *Crotalus durissus terrificus* snake venom, *Biochimie* 95 (2013) 2365–2375, <https://doi.org/10.1016/j.biochi.2013.08.028>.
- [65] S.P. Kanaujia, K. Sekar, Structures and molecular-dynamics studies of three active-site mutants of bovine pancreatic phospholipase A 2, *Acta Crystallogr. D Biol. Crystallogr.* 64 (2008) 1003–1011, <https://doi.org/10.1107/S0907444908022713>.
- [66] D.L. Scott, S.P. White, Z. Otwinowski, W. Yuan, M.H. Gelb, P.B. Sigler, Interfacial catalysis: the mechanism of phospholipase A 2, *Science* 250 (1990) 1541–1546, <https://doi.org/10.1126/science.2274785>.
- [67] C.L. Wee, K. Balali-Mood, D. Gavaghan, M.S.P. Sansom, The interaction of phospholipase A₂ with a phospholipid bilayer: coarse-grained molecular dynamics simulations, *Biophys. J.* 95 (2008) 1649–1657, <https://doi.org/10.1529/biophysj.107.123190>.
- [68] J.P. Zuliani, J.M. Gutiérrez, L.L. Casais e Silva, S. Coccuzzo Sampaio, B. Lomonte, C.F. Pereira Teixeira, Activation of cellular functions in macrophages by venom secretory Asp-49 and Lys-49 phospholipases A₂, *Toxicon* 46 (2005) 523–532, <https://doi.org/10.1016/j.toxicon.2005.06.017>.
- [69] D.A. Lauffenburger, A.F. Horwitz, Cell migration: a physically integrated molecular process, *Cell* 84 (1996) 359–369, [https://doi.org/10.1016/S0092-8674\(00\)81280-5](https://doi.org/10.1016/S0092-8674(00)81280-5).
- [70] C. Díaz, L. Valverde, O. Brenes, A. Rucavado, J.M. Gutiérrez, Characterization of events associated with apoptosis/anoikis induced by snake venom metalloproteinase BaP1 on human endothelial cells, *J. Cell. Biochem.* 94 (2005) 520–528, <https://doi.org/10.1002/jcb.20322>.
- [71] D.C. Aché, M.S.R. Gomes, D.L.N. Souza, M.A. Silva, M.I.H. Brandeburgo, K.A. G. Yoneyama, R.S. Rodrigues, M.H. Borges, D.S. Lopes, V.M. Rodrigues, Biochemical properties of a new PI SVMP from *Bothrops pauloensis*: inhibition of cell adhesion and angiogenesis, *Int. J. Biol. Macromol.* 72 (2015) 445–453, <https://doi.org/10.1016/j.ijbiomac.2014.08.050>.
- [72] R.C.A. Cedro, D.L. Menaldo, T.R. Costa, K.F. Zoccal, M.A. Sartim, N.A. Santos-Filho, L.H. Faccioli, S.V. Sampaio, Cytotoxic and inflammatory potential of the phospholipase A₂ from *Bothrops jararaca* snake venom, *J. Venom Anim. Toxins Incl. Trop. Dis.* 24 (2018 Nov 23) 33, <https://doi.org/10.1186/s40409-018-0170-Y>.
- [73] J.C. de Albuquerque Modesto, P.J. Spencer, M. Fritzen, R.C. Valença, M.L.V. Oliva, M.B. da Silva, et al., BE-I-PLA₂, a novel acidic phospholipase A₂ from *Bothrops erythromelas* venom: isolation, cloning and characterization as potent antiplatelet and inducer of prostaglandin I₂ release by endothelial cells, *Biochem. Pharmacol.* 72 (3) (2006) 377–384, <https://doi.org/10.1016/j.bcp.2006.04.032>.
- [74] D.C. Nunes, R.S. Rodrigues, M.N. Lucena, C.T. Cologna, A.C. Oliveira, A. Hamaguchi, et al., Isolation and functional characterization of proinflammatory acidic phospholipase A₂ from *Bothrops leucurus* snake venom, *Comp. Biochem. Physiol. C Toxicol. Pharmacol.* 154 (3) (2011) 226–233, <https://doi.org/10.1016/j.cbpc.2011.06.003>.
- [75] P.G. Roberto, S. Kashima, S. Marcussi, J.O. Pereira, S. Astolfi-Filho, A. Nomizo, et al., Cloning and identification of a complete cDNA coding for a bactericidal and antitumoral acidic phospholipase A₂ from *Bothrops jararacussu* venom, *Protein J.* 23 (4) (2004) 273–285, <https://doi.org/10.1023/b:joep.0000027852.92208.60>.
- [76] N.A. Santos-Filho, L.B. Silveira, C.Z. Oliveira, C.P. Bernardes, D.L. Menaldo, A. L. Fuly, et al., A new acidic myotoxic, anti-platelet and prostaglandin I₂ inducer phospholipase A₂ isolated from *Bothrops moojeni* snake venom, *Toxicon* 52 (8) (2008) 908–917, <https://doi.org/10.1016/j.toxicon.2008.08.020>.
- [77] T.R. Costa, D.L. Menaldo, C.Z. Oliveira, N.A. Santos-Filho, S.S. Teixeira, A. Nomizo, et al., Myotoxic phospholipases A₂ isolated from *Bothrops brazili* snake venom and synthetic peptides derived from their C-terminal region: cytotoxic effect on microorganism and tumor cells, *Peptides* 29 (10) (2008) 1645–1656, <https://doi.org/10.1016/j.peptides.2008.05.021>.
- [78] O. Brenes, E. Muñoz, R. Roldan-Rodríguez, C. Díaz, Cell death induced by *Bothrops asper* snake venom metalloproteinase on endothelial and other cell lines, *Exp. Mol. Pathol.* 88 (2010) 424–432, <https://doi.org/10.1016/j.yexmp.2010.02.002>.
- [79] A.T.B. Franco, L.M.G. Silva, M.S. Costa, S.F. Zamuner, R.P. Vieira, et al., Effect of photobiomodulation on endothelial cell exposed to *Bothrops jararaca* venom, *laser Med. Sci.* 31 (2016) 1017–1025, <https://doi.org/10.1007/s10103-016-1941-8>.
- [80] L.H. Gremiski, O.M. Chaim, K.S. Paludo, Y.B. Sade, M.F. Otuki, M. Richardson, W. Gremiski, E.F. Sanchez, S.S. Veiga, Cytotoxic, thrombolytic and edematogenic activities of leucurolysin-a, a metalloproteinase from *Bothrops leucurus* snake venom, *Toxicon* 50 (2017) 120–134, <https://doi.org/10.1016/j.toxicon.2007.03.002>.

- [81] B. Lomonte, J.M. Gutierrez, G. Borkow, M. Ovidia, A. Tarkowski, L.Å. Hanson, Activity of hemorrhagic metalloproteinase BAH-1 and myotoxin II from *Bothrops asper* snake venom on capillary endothelial cells *in vitro*, *Toxicon* 32 (1994) 505–510, [https://doi.org/10.1016/0041-0101\(94\)90302-6](https://doi.org/10.1016/0041-0101(94)90302-6).
- [82] P.K. Dos Santos, W.F. Altei, T.M. Danilucci, R.L.B. Lino, B.C. Pachane, A.C. C. Nunes, H.S. Selistre-de-Araujo, Alternagin-C (ALT-C), a disintegrin-like protein, attenuates alpha2beta1 integrin and VEGF receptor 2 signaling resulting in angiogenesis inhibition, *Biochimie* 174 (2020) 144–158, <https://doi.org/10.1016/j.biochi.2020.04.023>.
- [83] T. Iskratsch, H. Wolfenson, M.P. Sheetz, Appreciating force and shape—the rise of mechanotransduction in cell biology, *Nat. Rev. Mol. Cell Biol.* 15 (2014) 1–9, <https://doi.org/10.1038/nrm3903>.
- [84] H. Wolfenson, B. Yang, M.P. Sheetz, Steps in mechanotransduction pathways that control cell morphology, *Annu. Rev. Physiol.* 81 (2018) 1–21, <https://doi.org/10.1146/annurev-physiol-021317-121245>.
- [85] C.M. De Andrade, F.M. Rey, A.C.O. Cintra, S.V. Sampaio, M.R. Torqueti, Effects of crotoxin, a neurotoxin from *Crotalus durissus terrificus* snake venom, on human endothelial cells, *Int. J. Biol. Macromol.* 134 (2019) 613–621, <https://doi.org/10.1016/j.ijbiomac.2019.05.019>.
- [86] V. Ranta, A. Orpana, O. Carpen, U. Turpeinen, O. Ylikorkala, L. Viinikka, Human vascular endothelial cells produce tumor necrosis factor- α in response to proinflammatory cytokine stimulation, *Crit. Care Med.* 27 (1999) 2184–2187, <https://doi.org/10.1097/00003246-199910000-00019>.
- [87] B. Lomonte, Lys49 myotoxins, secreted phospholipase A₂-like proteins of viperid venoms: A comprehensive review, *Toxicon* 224 (2023) 107024, <https://doi.org/10.1016/j.toxicon.2023.107024>.